2015

Characterization of Fillite as a Planetary Soil Simulant in Support of Rover Mobility Assessment in High-Sinkage/High-Slip Environments

Michael Edwards
University of Vermont

CHARACTERIZATION OF FILLITE AS A PLANETARY SOIL SIMULANT IN SUPPORT OF ROVER MOBILITY ASSESSMENT IN HIGH-SINKAGE/HIGH-SLIP ENVIRONMENTS

A Thesis Presented

by

Michael Edwards

to

The Faculty of the Graduate College

of

The University of Vermont

In Partial Fulfillment of the Requirements
for the Degree of Master of Science
Specializing in Mechanical Engineering

January, 2015

Defense Date: August 13, 2014
Thesis Examination Committee:

Mandar Dewoolkar, Ph.D., Advisor
Dryver Huston, Ph.D., Advisor
Ehsan Ghazanfari, Ph.D., P.E., Chairperson
Darren Hitt, Ph.D.
Cynthia Forehand, Ph.D., Dean of the Graduate College

ABSTRACT

This thesis presents the results of a research program characterizing a soil simulant called Fillite, which is composed of alumino-silicate hollow microspheres harvested from the pulverized fuel ash of coal-fired power plants. Fillite is available in large quantities at a reasonable cost and it is chemically inert. Fillite has been selected by the National Aeronautics and Space Administration (NASA) Glenn Research Center to simulate high-sinkage/high-slip environment in a large test bed such as the ones encountered by the Spirit rover on Mars in 2009 when it became entrapped in a pocket of soft, loose regolith on Mars. The terms high-sinkage and high-slip used here describe the interaction of soils with typical rover wheels. High-sinkage refers to a wheel sinking with little to no applied force while high-slip refers to a spinning wheel with minimal traction.

Standard material properties (density, specific gravity, compression index, Young's modulus, and Poisson's ratio) of Fillite were determined from a series of laboratory tests conducted in general accordance with ASTM standards. Tests were also performed to determine some less standard material properties of Fillite such as the small strain shear wave velocity, maximum shear modulus, and several pressure-sinkage parameters for use in pressure-sinkage models. The experiments include an extensive series of triaxial compression tests, bender element tests, and normal and shear bevameter tests.

The unit weight of Fillite on Earth ranges between 3.9 and 4.8 kN/m^3, which is similar to that of Martian regolith (about 3.7 – 5.6 kN/m^3) on Mars and close to the range of the unit weight of lunar regolith (about 1.4 – 2.9 kN/m^3) on the Moon. The data presented here support that Fillite has many physical and mechanical properties that are similar to what is known about Martian regolith. These properties are also comparable to lunar regolith. Fillite is quite dilatant; its peak and critical angles of internal friction are smaller than those of most other simulants. Smaller shear strength, coupled with much smaller bulk unit weight as compared to other simulants, results in smaller bearing and shearing resistances allowing for better simulation of the intended high-sinkage, high-slip behavior for rover mobility studies.

The results of the normal bevameter tests were used to determine parameters for two models available in the literature - the Bekker model and the New Model of Mobility (N2M) model. These parameters were then used to predict the sinkage of a Spirit rover wheel if the rover were to be used on Fillite. The predicted sinkage of a Spirit rover wheel in Fillite was 84% of the wheel diameter, which was within the observed sinkage of 50 to 90% of the wheel diameter of the Spirit rover on Mars. Shear bevameter tests were also performed on Fillite to assess the shear stresses and shear deformations imparted by wheels under torsional loads. The results compared well to the estimated shear stresses and deformations of Martian soil caused by the wheels of the Spirit rover. When compared to other simulants (e.g. GRC-1), the pressure-sinkage and shear stress-shear deformation behaviors of Fillite confirm that Fillite is more suitable for high-sinkage and high-slip rover studies than other typical simulants derived from natural terrestrial soils and rocks.

ACKNOWLEDGEMENTS

I would like to acknowledge Mandar Dewoolkar and Dryver Huston for guiding me through this research process. They spent many hours with me to ensure I was producing the best work possible and I could not have completed my thesis without their help.

Thank you to Darren Hitt and the Vermont Space Grant Consortium for providing me with a NASA fellowship. It was a tremendous opportunity that not only aided in the completion of my masters but also provided great experiences within the fields of space science and engineering.

Lastly I would like to thank my family and friends that have not only supported me through my masters, but through my entire academic career as well. I would not have gotten as far as I have without them and I feel extremely grateful.

TABLE OF CONTENTS

Page

LIST OF TABLES

LIST OF FIGURES

CHAPTER 1: INTRODUCTION

Every rover that gets sent to an extraterrestrial body is tasked with a specific set of mission objectives. These objectives typically involve the use of onboard components to perform as expected for the duration of the mission timeline. This requires that the rover must remain mobile and operable throughout this timeframe for the mission. Designing rovers often involve physical model experiments in test beds of simulant soils on Earth.

The focus of most simulant development efforts has been to match physical properties of the soil on the intended planetary body. Most recently these have been Mars and the Moon. Inevitably, it is not possible to match all physical properties. Instead, compromises that partially match the physical properties are necessary. Soil simulants such as MMS Mars simulant and GRC-1 lunar simulant have matched properties such as the grain size distribution and bulk densities of their respective regoliths that they are trying to simulate. However, consider the property of bulk unit weight. The bulk unit weight of a material is its bulk weight per unit volume and is expressed as ρg, where ρ is the bulk density and g is the gravitational acceleration it experiences. The average bulk density of Martian soil is approximately 1,400 kg/m^3 resulting in a bulk unit weight of about 5.195 kN/m^3 on Mars. A material with that exact same density on Earth would have a bulk unit weight of 13.72 kN/m^3, because the gravity on Earth is 2.64 times that of Mars. Therefore, a material with the same density will weigh 2.64 times less on Mars than on Earth. This results in much higher confining pressures in simulation beds on Earth. The strength and stiffness of soils are highly dependent on confining pressures, which would then be not replicated correctly in the physical models.

On May 1st 2009, the Spirit Rover became stuck in a pocket of Iron (III) Sulfate near the Home Plate plateau of Mars that was hidden under a layer of normal looking soil (NASA, 2009). Spirit was physically unable to free itself from the soft, loose soil, which ultimately led to its abandonment. It should be noted that Spirit successfully operated for over five years and its counterpart Opportunity continues to operate successfully to this day. The Curiosity rover, which touched down in 2012, also continues to operate smoothly. The surface of Mars is a combination of fine sand-like material, clods, rocks and boulders. The capabilities to simulate the majority of these conditions exist on Earth. The one small, but potentially very important area that seems to be lacking is the ability to simulate high-sinkage/high-slip conditions. These conditions are rare for a rover to encounter but could cause its demise if unprepared.

To better prepare for challenges such as these, rover mobility experiments are being conducted at NASA laboratories and elsewhere. NASA Glenn Research Center has developed a "Sink Tank", which is a large container (12 m long by 3 m wide by 0.5 m deep) that can be filled with any simulant. The purpose of the Sink Tank is to produce conditions under which most vehicles would become immobilized using conventional driving techniques. Selecting an appropriate granular material that can simulate this mobility challenge on the Moon or Mars is critical. NASA Glenn Research Center recently selected a granular material called Fillite (Tolsa USA Inc., 2014) for three reasons (Creager, personal communication, June 2014). First, Fillite appeared to allow laboratory simulation of high-sinkage, high-slip type environment, similar to what was encountered by Spirit and other rovers. Second, Fillite is non-hazardous and can be obtained in large quantities and a reasonable cost. Third, Fillite is granular. Its particle

sizes and unit weight are comparable to the regolith on Mars, and are reasonably close to the regolith on the Moon. This paper presents geotechnical characterization on Fillite.

Fillite is a product of Tolsa USA Inc. and is described as a glass hard, free flowing additive typically used for reducing the weight of cement and resins (Tolsa USA Inc., 2014). The bulk density of the Fillite used (grade 500W-LF, off-white in color) is listed as 0.4 – 0.49 g/cm^3 which would give it a bulk unit weight approximately equal to that of the loose, drift soil that blankets the surface of Mars.

The objectives of the work presented here were to:

1) determine index properties of Fillite such as specific gravity, minimum and maximum bulk density, and grain size distribution;
2) determine mechanical properties of Fillite such as cohesion, internal friction angle, Young's modulus, Poisson's ratio and small-strain shear modulus as a function of bulk density and confining stress;
3) determine pressure-sinkage behavior of Fillite and material parameters for commonly used pressure-sinkage models and assess actual rover behavior; and
4) assess if Fillite is a suitable simulant for high-sinkage, high-slip rover mobility testing.

The results for Fillite obtained here are compared to what is known about Martian soil as well as lunar soil, as many of the challenges presented with traversing the surface of Mars are also present for the surface of the Moon as well.

This thesis is organized as follows. This introduction chapter is followed by a chapter on the geotechnical properties of Fillite, which is written in a manuscript format, intended for submission to the Journal of Aerospace Engineering. This manuscript is

followed by a second manuscript on the pressure-sinkage behavior of Fillite intended for submission to the Journal of Terramechanics. The last chapter presents overall conclusions and recommendations for future work. Appendices present summaries of cone penetration tests as well as details of test procedures employed in this work.

References

McKee, M. (2009). "Mars rover may not escape sand trap for weeks". *New Scientist*. May 12, 2009.

NASA (2009), "*Spirit and Opportunity Mission News"*, http://www.nasa.gov/mission_pages/mer/freespirit.html. Last accessed August 6, 2014.

Tolsa USA Inc. (2014), http://www.thecarycompany.com/products/Tolsa/tolsa-usa-inc-fillite.html, last accessed: July 5,2014

CHAPTER 2: GEOTECHNICAL PROPERTIES OF FILLITE - A SIMULANT FOR PLANETARY HIGH-SLIP/HIGH-SINKAGE ROVER MOBILITY STUDIES

2.1. Abstract

Physical model studies on rovers are conducted first on Earth, often on granular simulants, before they are deployed to Mars, the Moon, or other planetary bodies. Researchers at the NASA Glenn Research Center developed a large test bed called the "sink tank" specifically to simulate rover mobility in high-sinkage, high-slip situations similar to the ones encountered by the Spirit rover on Mars. For the test bed, they selected a granular material called Fillite, which is composed of alumino-silicate hollow microspheres harvested from the pulverized fuel ash of coal-fired power plants. Fillite is available in large quantities at a reasonable cost and it is chemically inert. The particle size distribution of Fillite (grade 500W-LF, off-white in color, made by Tolsa USA Inc.) is uniform with particles ranging mostly between 0.075 mm and 0.42 mm (mean particle size of about 0.2 mm). Its unit weight on Earth is 3.9 – 4.8 kN/m^3. This is similar to that of Martian regolith on Mars (about 3.7 – 5.6 kN/m^3) and close to the range of the unit weight of lunar regolith on the Moon (about 1.4 – 2.9 kN/m^3). The focus of the work presented in this paper is to summarize geotechnical characterization of Fillite, specifically its mechanical properties such as shear strength parameters, elastic modulus, Poisson's ratio and small-strain shear modulus. These properties of Fillite are compared to the known and estimated properties of Martian and lunar regoliths as well as of other commonly used simulants. The data presented here support that Fillite has many physical and mechanical properties that are similar to what is known about Martian regolith. These

properties are also comparable to lunar regolith. Fillite is quite dilatant; its peak and critical angles of internal friction are smaller than those of most other simulants. Smaller shear strength, coupled with much smaller bulk unit weight as compared to other simulants, results in smaller bearing and shearing resistances allowing for better simulation of the intended high-sinkage, high-slip behavior for rover mobility studies.

2.2 Introduction

The National Aeronautics and Space Administration (NASA)'s interest in exploring Mars and the Moon, both with robots and humans, has driven the development of materials and facilities that can reliably mimic specific conditions of interest on Martian and lunar surfaces in laboratory studies conducted on Earth. Test beds that mimic features of the terrains on Mars and the Moon are essential to designing vehicles and structures that are fully capable of operating successfully once they reach their destinations. On May 1st 2009, the Spirit Rover became stuck in a pocket of Iron (III) Sulfate near the Home Plate plateau of Mars that was hidden under a layer of normal looking soil (NASA, 2009). Spirit was physically unable to free itself from the soft, loose soil, which ultimately led to its abandonment. To better prepare for challenges such as these, rover mobility experiments are being conducted at NASA laboratories and elsewhere. NASA Glenn Research Center has developed a "Sink Tank", which is a large container (12 m long by 3 m wide by 0.5 m deep) that can be filled with any simulant. The purpose of the Sink Tank is to produce conditions under which most vehicles would become immobilized using conventional driving techniques. Selecting an appropriate granular material that can simulate this mobility challenge on the Moon or Mars is

critical. NASA Glenn Research Center recently selected a granular material called Fillite (Tolsa USA Inc., 2014) for three reasons (Creager, personal communication, June 2014). First, Fillite appears to allow laboratory simulation of high-sinkage, high-slip type behavior, similar to what was encountered by Spirit and other rovers. Second, Fillite is non-hazardous and can be obtained in large quantities and a reasonable cost. Third, Fillite is granular, its particle sizes and unit weight are comparable to the regolith on Mars, and are reasonably close to the regolith on the Moon. This paper presents geotechnical characterization of Fillite.

The majority of the data about the physical properties of Martian soils have been derived from orbital or remote observations and experiments that were performed by past Mars rovers and landers. Martian surface materials have been categorized into five types - drift material, clods and rusts, blocky material, rocks, and features thought to be outcrops of bedrock (Moore, et al., 1982; Stoker, et al. 1993). Since the explorations on Mars have largely revealed only photographs and remote sensing of its surface features, these observations have been used to infer mechanical properties of Martian regolith. For example, Sullivan, et al. (2011) analyzed wheel trenches and wheel scuffs from photographs to infer shear strength properties (cohesion and internal friction angle) of Martian regolith. In comparison, more details are known about lunar regolith. Nearly the entire lunar surface is covered with a layer of fragmented and unconsolidated rock material that blankets the underlying bedrock (Heiken et al, 1991). This layer of loose material is referred to as the lunar regolith. The thickness of the regolith varies depending on the terrain, but on average it is between 10–15 m in the rough and heavily cratered highlands and 4–5 m in the relatively smooth mare regions (Heiken et al. 1991).

In general the lunar regolith is described as "a somewhat cohesive, dark grey to light grey, very fine-grained, loose, clastic material derived primarily from the mechanical disintegration of basaltic and anorthositic rocks" (Heiken et al. 1991). Unfortunately, a very limited quantity of lunar regolith has been returned to Earth and Martian regolith has not been brought to Earth, which has prevented their comprehensive geotechnical testing. Therefore, several simulants of lunar and Martian regoliths have been developed.

For sinkage mobility type tests, simulants are required to satisfy the following requirements (e.g. Li, et al., 2013): (1) mechanical properties (strength and stiffness) of the simulant relevant to the wheel-soil-interaction need to be similar to that of the Martian or lunar regoliths; (2) a large quantity of the simulant can be produced at a relatively low cost; (3) the simulant needs to be environmental friendly and non-hazardous so that researchers can have easy access to the testing site; (4) the simulant is durable enough so repeatable use is possible; and (5) the unit weight of the simulant can be controlled in the range of that of typical Martian and/or lunar regolith.

One of the most commonly used lunar simulants is JSC-1A, which was developed by NASA's Johnson Space Center to replicate a low-titanium lunar mare regolith (Alshibli and Hasan, 2009). In addition, coarse and fine variations JSC-1AC and JSC-1AF were made to represent the coarser and dust components of the lunar regolith. However, JSC-1A, JSC-1AC, and JSC-1AF are only available in limited quantities. Other simulants include the NU-LHT series of lunar highland regolith simulants (i.e. NU-LHT-1M, NU-LHT-1D, NU-LHT-2M, and NU-LHT-2C), the Canadian highland simulants OB-1 and CHENOBI, and the Chinese mare simulant NAO-1 and mare simulant CAS-1. Several extinct simulants are JSC-1, a precursor to JSC-1A; MLS-1 and

MLS-2, mare and highland simulants, respectively, developed by the University of Minnesota; and the Japan Aerospace Agency's simulant FJS-1 (Edmunson et al. 2010). A relatively newer lunar simulant developed for tractive performance studies of lunar vehicles is GRC-1, which is a prescribed mixture of four different sands to a particle size distribution similar to coarse fraction of lunar soil and can be prepared in large quantities at a cost 100 times less than other lunar soil simulants (Oravec, et al., 2010). Another relatively new lunar simulant is GRC-3, which is composed of Bonnie silt (a natural loess excavated from a site in Burlington, CO, and four types of sands from the Best Sand Corporation of Chardon, OH (BS 110, BS 565, BS 620, and BS 2040) (He, et al., 2011). Since all of the soils are commercially available at relatively low cost, it is possible to make large quantities of GRC-3 at a reasonable price. A number of Martian simulants have also been developed (e.g. Seiferlin, et al., 2008). For example, simulants JSC Mars-1, Salten Skov, and MMS have been developed, which are mostly made using terrestrial soils. JSC Mars-1 is a simulant that is less than 1 mm size fraction of a palagonitic tephra (glassy volcanic ash altered at low temperatures). The material was collected from the Pu'u Nene cinder cone, located in the saddle between Mauna Loa and Mauna Kea volcanoes on the Island of Hawaii (Allen, et al., 1997).

Many of the above simulants match estimated and/or measured physical properties such as density, grain size, friction angle, and cohesion of Martian and lunar regoliths; however, they may not be suitable for sinkage simulations. The strength and stiffness of soils depend on the effective confining stress, which itself is induced by self-weight of the soil. Therefore, unit weight of the simulant ideally should be in the range of a typical Martian or lunar regolith. Since the gravity on the Moon and Mars is

approximately 1/6th and 3/8th of that on Earth, respectively, the bulk unit weight of the simulant also needs to be 1/6th to 3/8th of a typical soil. A few efforts have recently been made to develop light-weight simulants. For example, the simulant CWRU1 was developed specifically for high-sinkage testing by mixing lunar simulant GRC-3 with small Styrofoam balls to lighten the weight (Li et al, 2013). While CWRU1 was able to achieve relatively low densities, grain sizes were limited to 2-4 mm which is significantly larger than most Martian soils. The Styrofoam also has a tendency to deform under load, possibly affecting its mechanical behavior under changing loads.

As mentioned earlier, NASA Glenn Research Center has selected a material called Fillite for their sink tank, which is a focus of this paper. Fillite (Tolsa USA Inc., 2014) is composed of alumino-silicate hollow microspheres and is harvested from the pulverized fuel ash of coal-fired power plants. It is a light, granular material that is also chemically inert, free flowing and with strong particles (Tolsa USA Inc., 2014). Fillite is used in several industrial applications where it is added to cement or an epoxy resin to provide both strength and a reduction in weight. Fillite (grade 500W-LF, off-white in color) used in this investigation and also used in the sink tank at NASA Glenn Research Center was obtained from Tolsa USA Inc. According to the supplier (Tolsa USA Inc., 2014), this Fillite has 34 - 40% alumina (as Al_2O_3), 55 – 65% of silica (as SiO_2) and maximum of 2% iron (as Fe_2O_3). Other relevant properties reported by the supplier are summarized in Table 2.1. The bulk density of Fillite reported by the supplier is 0.4 – 0.49 g/cm^3 resulting in a bulk unit weight (on Earth) of about 3.9 – 4.8 kN/m^3, which is similar to that of Martian regolith (about 3.7 – 5.6 kN/m^3; the gravitational acceleration on Mars is 3.722 m/s^2 as opposed to 9.807 m/s^2 on Earth). Although the bulk unit weight of lunar

regolith is about 1.4 – 2.9 kN/m^3, somewhat less than that of Fillite, the results of rover mobility experiments conducted on Fillite should be applicable for planning rover mobility on lunar terrain.

This paper summarizes the index and mechanical properties of Fillite including grain size distribution, maximum and minimum bulk densities, shear strength parameters, Young's modulus, Poisson's ratio, compression and recompression indices and small-strain shear modulus. The employed test methods are presented and the material properties are compared to available and estimated material properties of lunar and Martian regoliths and select simulants and expected mechanical behavior of a typical granular soil (e.g. clean sands) whenever possible.

2.3 Laboratory Testing Program

A series of laboratory tests were conducted on Fillite to determine its geotechnical properties, including specific gravity, grain size distribution, minimum and maximum bulk densities, shear strength parameters (cohesion and internal friction angle), dilatancy angle, Young's modulus, Poisson's ratio, compression and recompression indices, and small-strain shear wave velocity and shear modulus. The strength and stiffness properties were determined at four different densities and four different confining pressures. These laboratory tests were conducted in general accordance with ASTM standards, when available, which are summarized in Table 2.2.

2.4 Physical Properties of Fillite

A visual inspection of Fillite particles was conducted with a Scanning Electron Microscope (SEM) to reveal their surface texture and overall shape. Example images appear in Figures 1a and b, which reveal that Fillite particles are spherical and uniform in size and shape. Figure 1c shows a close-up of Fillite particles that were forcefully broken. The hollow structure of Fillite spheres can be seen in Figure 1c. In this investigation, previously unused or previously gently handled Fillite was used for all testing.

A grain size distribution of Fillite was also determined in general accordance with ASTM D6913. The analysis was conducted on three random samples of Fillite, each 1,000 g in mass. Sieves of sizes 40, 60, 80, 100, 140, 170, and 200 were used to determine the grain size range. The results of the sieve analysis are shown in Figure 2. 98% of Fillite particles by mass were larger than 0.075 mm and smaller than 0.42 mm.

The grain size distributions in Figure 2 were used to determine the diameters of Fillite particles corresponding to sizes such that 10%, 30%, 50% and 60% of particles are smaller by mass: effective size, D_{10} = 0.13 mm; D_{30} = 0.2 mm; mean diameter D_{50} = 0.203 mm; and D_{60} = 0.21 mm, respectively. The coefficient of uniformity C_u (= D_{60}/D_{10}) and the coefficient of curvature C_c (= $D^2_{30}/[D_{60} \times D_{10}]$) were then determined to be 1.62 and 1.47, respectively. Based on these numbers Fillite can be classified as a "poorly graded sand (SP)" according to the Unified Soil Classification System (USCS).

The specific gravity (G_s), which is the comparison of the density of soil particles to pure water at 4˚C, was determined in general accordance to ASTM D854. This value was determined to be 0.67, which is between three and four times smaller than other simulants, including lunar simulants.

The state of density of a dry granular soil is typically represented in terms of its maximum and minimum possible bulk densities using a parameter called relative density (D_r) which is expressed as:

$$D_r = \frac{\rho-\rho_{min}}{\rho_{max}-\rho_{min}} \cdot \frac{\rho_{max}}{\rho} \cdot 100 \quad (1)$$

where ρ is the measured bulk density of a given state of a soil, ρ_{min} is the minimum bulk density of the soil, and ρ_{max} is the maximum bulk density of the soil. The values of ρ_{max} and ρ_{min} were determined by performing maximum and minimum density tests per standards ASTM D4253 and ASTM D4254, respectively. Three separate tests were done for each standard.

Void ratio is an index property of a soil, which is defined as the volume of voids divided by the volume of solid particles. The maximum and minimum void ratios (e_{max} and e_{min}) were then calculated using the values of specific gravity and minimum and maximum densities, respectively, as follows:

$$e = \frac{G_s\rho_w}{\rho_d} - 1 \quad (2)$$

where ρ_w is the density of water (1 g/cm^3). Porosity is another index property of a soil, which is defined as the volume of voids divided by the total volume of the soil and can be calculated using void ratio as follows:

$$n = \frac{e}{1+e} \quad (3)$$

Minimum and maximum porosities were then calculated from the maximum and minimum void ratios, respectively.

Table 2.3 contains a summary of the determined index properties of Fillite.

2.5 Compressibility of Fillite

Compressibility of a soil is an important property as it relates to how the material compresses under a load. Whether it is designing a rover, excavation equipment, or a permanent structure, this property will be relevant. The soil compressibility parameters for Fillite were determined by conducting the one-dimensional compression test in general accordance to ASTM D2435 where a series of vertical, centric loads are applied to the specimen, which is restricted from deforming laterally. The change in specimen height is recorded following each load increment. The recorded change in specimen height is used to compute the changes in void ratio. Figure 3 summarizes the results plotted as the void ratio versus the logarithm of vertical stress. The slope of the straight line portion of the curve is known as the compression index (c_c) and is calculated as:

$$c_c = \frac{e_1 - e_2}{\log\frac{p_2}{p_1}} \tag{4}$$

where e_1 and e_2 correspond to the void ratios of the soil at the vertical stresses p_1 and p_2, respectively. The sample was then slowly unloaded using the same loading increments but in reverse order. This produces a recompression curve that does not follow the first curve, but typically remains below it with a much flatter slope. The same procedure for finding the compression index can also be used for finding the recompression index (c_r) which is determined as:

$$c_r = \frac{e_1 - e_2}{\log\frac{p_2}{p_1}} \tag{5}$$

where e_1 and e_2 correspond to the void ratios of the soil at the vertical stresses p_1 and p_2 on the recompression curve.

From the plots in Figure 3 the compression and recompression indices of Fillite were calculated as 0.041 and 0.014, respectively, by averaging the values across the three tests. While no compression properties are currently available for Martian regolith, these values are comparable to lunar regolith. According to the Lunar Sourcebook (Heiken et. al, 1991), the compression and recompression indices as determined by the Apollo 12 mission ranged between 0.03 to 0.108 and 0 to 0.013, respectively. Fillite falls within this range for compression index values and is approximately equal to the largest recompression index reported.

2.6 Triaxial Compression Testing on Fillite

The bulk of the mechanical properties of Fillite were determined from a series of strain-controlled, consolidated drained (on dry specimens) triaxial compression tests using the Geocomp LoadTrack II triaxial equipment. A total of sixteen triaxial tests were conducted with four densities and four confining pressures.

The triaxial test specimens (7.2 cm in diameter and about 15 cm in height) were prepared at four target relative densities (about 20, 40, 60 and 75%). The specimens were constructed in nine layers using a triaxial split mold. The density was controlled by measuring the mass of each layer of Fillite, then gently tamping each layer to achieve a desired volume. Controlling the volume of each layer was a bit tricky because Fillite tends to displace away from the point of contact instead of compacting with other particles. Even applying a small force to a flat surface of Fillite is enough to cause it to displace unevenly. This caused some problems for preparing samples denser than 40% relative density. To overcome this, a mechanical vibrator setup was constructed. This

arrangement utilized a sine wave generator and a mechanical vibrator to apply vibrations to the side of the metal mold. This caused Fillite to settle to a desired higher density and also uniformly. The amplitude of vibration was adjusted to control the amount of settling.

When the desired amount of Fillite was added, a vacuum was pulled within the sample to give it enough rigidity to stand on its own. The applied vacuum was always less than the intended confining pressure. An external pressure chamber was then placed around the specimen. The chamber was filled with de-aired water very carefully so as not to form any air bubbles. This water was then pressurized to desired level of confining pressure (σ_3). The change in the volume of water in the confining chamber was tracked because it essentially provides the volume change of the specimen, which is then used to determine volumetric strain of the specimen during testing.

The actual relative densities of each specimen within a series were very close. The average relative densities (before the application of confining pressure) were 22.7, 39.3, 63.6 and 74.5%. All specimens were compressed at a constant displacement rate of 1.5 mm/min. The specimens were subjected to an unloading-reloading cycle at about 2% axial strain to enable computation of elastic Young's modulus, discussed later in the paper. Some tests were conducted twice to establish repeatability. The compression load was monitored using a loadcell and the axial deformation of the specimen was monitored using a linear variable differential transformer (LVDT). The axial deformation measurement was used to calculate the axial strain.

2.6.1 Stress-Strain Behavior

The data from the triaxial tests are summarized in the form of plots of deviator stress or the principal stress difference ($\sigma_1 - \sigma_3$) versus axial strain (ε_a) and volumetric

strain (ε_{vol}) versus axial strain in Figure 4. Specimens were grouped according to their relative density. A volume increase (dilation) is displayed as negative, where compression is positive. The deviator stress-axial strain plots show a gradual increase in deviator stress to a peak value followed by a small amount of softening which leads to a critical state condition. The amount of softening increases slightly with increased density. As expected, peak stress and critical stress both increase with confining pressure and density.

The volume change plots show that specimens exhibited an initial contraction, followed by dilation. As expected, similar to a granular soil, dilation decreased with the increasing confining pressure but increased with increasing density. In general, Fillite tended to dilate regardless of the density for the confining pressures investigated. This is somewhat different than typical natural sands as they typically tend to compress instead increase in volume at low densities. This is probably because Fillite particles are uniform in size and shape which does not facilitate grain rearrangement during shear, leading to dilation under shear.

Elastic (Young's) modulus (E) was also calculated from triaxial test results. As illustrated in Figure 5, the modulus can be calculated using the deviator stress versus axial strain plots in different ways: (1) the slope of the initial tangent of the initial loading curve (E_i), (2) the slope of the initial tangent to the reloading loop at zero deviator stress (E_r), (3) the slope of the line joining the bottom of the reload loop to the top of the unloading loop (also known as the unload-reload modulus of elasticity, (E_{ur}), and (4) the slope of the bottom tangent of the unloading loop (E_u). Methods 1, 2, and 4 require some judgment in deciding on the tangents, the third method is the most straightforward and is

not subjective. Therefore, the unload-reload moduli are reported here. The moduli values are summarized in Table 2.4. The elastic modulus as a function of confining stress and relative density of Fillite is plotted in Figure 6a. As expected, the elastic modulus increased with increased density and increased confining stress. The values of elastic modulus ranged from about 20 to 73 MPa. Typical values of elastic modulus for loose, medium and dense sands are expected to be between 5-10, 20-50, and 50-100 MPa respectively (Fang 1990). The elastic moduli of Fillite determined in this work are within this range.

An empirical predictive model was developed based on the relationship between elastic modulus, relative density, and confining pressure. As seen in Figure 6a, elastic modulus appears to increase more or less linearly with density and confining stress. A multi-variate linear regression was conducted resulting in the following empirical relationship:

$$E_{ur} = 2.74 + 0.284\sigma_3 + 0.386D_r \quad (6)$$

where E_{ur} is in MPa, σ_3 is confining pressure in kPa, and D_r is in percent. As seen in Figure 6b, this model is quite accurate with an R^2 value of 0.98 and can be used for predicting the unloading-reloading modulus of Fillite for conditions where the relative density (between about 20 and 75%) and confining pressure (between 25 and 150 kPa) are known.

Poisson's ratio (υ) was calculated using the relationship:

$$\nu = -\frac{\varepsilon_3}{\varepsilon_a} \quad (7)$$

where ε_3 is the radial strain, which is determined using the following equation:

$$\varepsilon_3 = \frac{\varepsilon_{vol} - \varepsilon_a}{2} \quad (8)$$

where ε_{vol} is the measured volumetric strain at the corresponding axial strain. The values of ε_a were the same values used for the determination of Young's modulus and the values of ε_{vol} were taken from the corresponding ε_a values and the volumetric strain curve. The range of Poisson's ratio was between 0.3 and 0.41. Typical values of Poisson's ratio for sands are expected to be between 0.10 to 0.40 respectively (Kulhway and Mayne, 1990). The Poisson's ratio of Fillite reported here are close to this range.

2.6.2 Shear Strength Parameters

Shear strength properties of a soil are very influential on vehicle performance, structure stability, excavations, etc. The parameters of cohesion and friction angle, which are the primary characteristics of shear strength, were determined from the series of triaxial tests presented above. Shear strength is most often characterized with the Mohr-Coulomb failure criterion, which is written as:

$$\tau_f = c + \sigma \, tan\phi \tag{9}$$

where τ_f is the shear stress of the material at failure along the failure plane; *c* is cohesion; ϕ is the angle of internal friction of the material; and σ is the normal stress on the failure plane. Equation 9 can also be expressed in terms of the major (σ_{1f}) and minor (σ_{3f}) principal stresses at failure as:

$$\sigma_{1f} = \sigma_{3f} \, tan^2\left(45^o + \frac{\phi}{2}\right) + 2\, c \tan\left(45^o + \frac{\phi}{2}\right) \tag{10}$$

As a minimum, triaxial tests done at two confining pressures are needed to determine c and ϕ from the slope of the tangent to the two Mohr circles assuming a linear Mohr-Coulomb failure envelope expressed by equation 10 above. In this test series, tests were conducted at four confining pressures. Figure 7 presents Mohr circles for both peak and

critical state conditions for all four relative densities. The plots also include corresponding peak (c_p and ϕ_p) and critical (c_{cs} and ϕ_{cs}) cohesion and friction angle, respectively. The "peak" designation indicates that the values were calculated for the highest stress condition on the stress-strain curve. "Critical state" indicates that the values were calculated at the final stress condition. In general, the ϕ_{cs} and c_{cs} were smaller than ϕ_p and c_p, as expected.

Over a wide range of confining pressures (25 – 150 kPa), some nonlinearity in the failure envelope is to be expected. The Mohr-Coulomb model does not account for the dilatancy of the material explicitly. This is a limitation of the model when it is used to describe the behavior of dilative granular material, such as Fillite. To incorporate the influence of dilatancy angle (ψ) explicitly into a friction-dilatancy model, ϕ_p and ϕ_{cs} were calculated by substituting cohesion (c) equal to zero in equation 9 and solving for ϕ. The corresponding secant friction angles for each relative densities used are plotted in Figure 8 as a function of confining pressure. A second degree polynomial fit was used to illustrate that the relation between the friction angle and confining pressure appears nonlinear.

The dilatancy angle ψ was determined using the following equation:

$$\psi = \sin^{-1}\left(-\frac{\frac{d\varepsilon_{vol}}{d\varepsilon_1}}{2+\frac{d\varepsilon_{vol}}{d\varepsilon_1}}\right) \tag{11}$$

where $d\varepsilon_1$ and $d\varepsilon_{vol}$ correspond to the slope of the ε_{vol} versus ε_1 relationship at the peak stress location (Vermeer and Schanz, 1996). The influence that confining pressure has on dilatancy angles is presented in Figure 9. A second degree polynomial fit was applied to this plot as well to illustrate a potentially non-linear relationship. Bolton (1986)

proposed a statistical model for sands that links ϕ_p and ϕ_{cs} for triaxial experiments as follows:

$$\phi_p - \phi_{cs} \approx 0.5\psi = 3I_R \quad (12a)$$

$$I_R = D_r\,(10 - \ln p') - 1 \quad (12b)$$

where I_R = empirical relative density index; p′ = mean effective stress at failure (kPa); and D_r is the relative density in percent. This model did not yield accurate predictions for dilatancy angle or peak friction angle for Fillite, the predicted values were too low. In order to improve this model for Fillite, the following relationships are proposed for ϕ_p and ψ:

$$\phi_p = \phi_{cs} + 0.57\frac{{D_r}^{0.38}}{{\sigma_3}^{0.15}} \quad (13\,a)$$

$$\psi = 3.95\frac{{D_r}^{0.58}}{{\sigma_3}^{0.23}} \quad (13\,b)$$

where D_r is expressed in percent and σ_3 is the initial confining pressure in kPa. These equations give good predictions for peak friction angles and dilatancy angle with R^2 of 0.94 and 0.95, respectively, as illustrated in Figure 10. Equations 13a and b can be used to predict the strength properties of Fillite for relative density between about 20% and 75% and confining pressure between 25 kPa and 150 kPa.

2.7 Small-Strain Shear Wave Velocity and Shear Modulus

The small-strain (strain amplitudes of the order of 10^{-4} or less) shear modulus of soils (G_{max}) is a parameter that is relevant in assessing wave propagation, foundations subjected to dynamic loadings and soil improvement. This small-strain shear modulus is related to shear wave velocity as:

$$G_{max} = \rho\, v_s^2 \quad (14)$$

where ρ and v_s are the bulk density and shear wave velocity of the soil.

The use of bender elements is a popular laboratory method for measuring shear wave velocity of a soil. A "bender element" is a small piezoelectric ceramic sensor made of two piezoelectric plates rigidly bonded together. One element transmits a signal and another to measures the transmitted signal at some known distance away. The shear wave velocity is computed as the distance traveled by the wave between the two bender elements divided by the travel time. The travel distance can be reasonably assumed as tip to tip distance between the transmitter and the receiver bender elements (Dyvik and Madshus, 1985, Viggiani and Atkinson, 1995, Chaney et al., 1996). However, finding travel time is typically not straightforward because the output signal is obscured by signal interference such as reflected waves from sides, near field effects, and cross talk (Lee and Santamarina, 2005). These effects have been extensively studied and many different methods such as using frequency domain, cross correlation, and signal matching have been suggested by Viggiani and Atkinson (1995) and Lee and Santamarina (2005). Here, a simpler and more commonly used method of selecting the arrival time from time domain was employed by using the first inversion point (also known as zero crossing) that precedes the first major peak of the transmitted wave.

A modified triaxial cell with specimen end caps fitted with bender elements (15.9 mm long, 6.4 mm wide and 0.51 mm thick) was used for shear wave velocity measurements. The Fillite specimens were prepared in the same manner as the triaxial tests and the same pressure chamber was used to regulate confining pressure.

The densities of the samples were kept similar to those of the triaxial tests with four relative densities of 24.0, 40.5, 62.0, and 76.0%. Confining pressure was increased

in increments (ranging from 12.5 to 150 kPa) and the shear wave velocity was measured after no further volume change was observed following each pressure increment. A sinusoidal wave with a fixed frequency ranging from 15 to 25 kHz was used for exciting the bender elements. These higher frequencies were chosen to reduce the interference that often arises from near field effects as well as from reflected waves from the boundary of the sample. It is a common observation that the measured shear wave velocity has some dependence on the frequency of excitation (Blewett et al., 2000). To reduce the variability in the results, the average shear wave velocity after neglecting the highest and lowest values is reported here. The shear wave velocities are summarized in Table 2.5 and plotted in Figure 11a. The shear wave velocity of a fine sand (similar to Fillite in grain size) is expected to be between 100 and 250 m/s (Sirles and Viksne, 1990). The measured shear wave velocities in Fillite are in this range.

Hardin and Richart (1963) suggested the following correlation for shear wave velocity based on their resonant column test results on Ottawa sand, which is a fine grained sand:

$$v_s = (19.7 - 9.06\, e)(\sigma_3)^{0.25} \quad \text{for } \sigma_3 \geq 95.8\, kPa \tag{15a}$$

$$v_s = (11.36 - 5.35\, e)(\sigma_3)^{0.3} \quad \text{for } \sigma_3 < 95.8\, kPa \tag{15b}$$

where σ_3 is the confining pressure in Pa, which gives v_s in m/s. Figure 11b compares the measured and predicted (using the above equation) shear wave velocities on a 1:1 plot. As is evident by the distribution around the 1:1 line, this model is not as accurate at predicting the shear wave velocity of Fillite with an R^2 value of 0.86 across each plot. A new shear wave velocity model for Fillite was developed empirically along the same lines as the Hardin and Richart (1963) model and is written as:

$$v_s = (119.8 - 85\,e)(\sigma_3)^{0.25} \text{ for } 25 \text{ kPa} \leq \sigma_3 \leq 150\,kPa \quad (16)$$

where σ_3 is in kPa. Comparing the predicted and measured velocities on a 1:1 plot with the new model reveals a much tighter distribution around the 1:1 line (Figure 11c) with an R^2 value of 0.94.

Some empirical relationships are available to estimate the maximum shear modulus of sands. For example, Hardin and Black (1968) suggested the following equation for round-grained sands:

$$G_{max} = \frac{6908\,(2.17-e)^2}{1+e}(\sigma_3^{0.5}) \quad (17)$$

Seed and Idriss (1970) suggested the following equation:

$$G_{max} = 218.82\,K_{2max}(\sigma_3^{0.5}) \quad (18)$$

where K_{2max} is an empirical parameter dependent on void ratio, e, and relative density, D_r. Both G_{max} and σ_3 in the above two equations are in kPa. It is to be noted that per equation 17, G_{max} is directly proportional to the bulk density of the material. The bulk density of Fillite is about 0.45 g/cm^3, which is only about 25% of that of typical sand. Therefore, the empirical correlations from equation 17 are not expected to compare very well with G_{max} of Fillite due to the fact that it uses void ratio instead of density. Void ratio depends on the geometry of the particles where density is dependent on the mass, so any empirical equation based on typical sands will not apply well to Fillite. The relationship between G_{max} varies between four and five times as large as the measured values, which were expected. Equation 18 was more accurate at predicting G_{max} because K_{2max} was determined specifically for Fillite based on the experimental results. This prediction model is presented in Figure 12 and is recommended for Fillite. Table 5 includes K_{2max} values for Fillite which are between 10.2 and 13.9. These are between 3 and 4 times

smaller than K_{2max} values for typical sand which generally range from 34 to 59 for D_r = 30 to 75% (Seed and Idriss, 1970). Alternatively, to estimate G_{max}, first v_s can be predicted using equation 16, then equation 14 can be used.

2.8 Conclusions

A series of laboratory tests were conducted to determine the geotechnical properties of the light-weight, granular material known as Fillite. These measurements will serve as the basis to determine whether Fillite is effective at mimicking mechanical properties of Martian regolith and soils of other low gravity celestial bodies, and particularly relevant to vehicle mobility studies. The test results for Fillite are summarized in Table 2.6 along with comparisons to what is known about Martian regolith, other Martian simulants, lunar soil, and popular lunar simulants. The following conclusions can be drawn based on the results presented here:

1. The particle size distribution of Fillite falls outside of the range of the loose drift material on Mars that was determined by Viking 1 but within the range of the blocky surface material. The drift material ranged from 0.0001 to 0.01 mm while the blocky material ranged from 0.0001 to 1.5 mm.
2. Although the specific gravity is not known for Martian regolith for comparison purposes, the unit weight of Fillite falls well within the range based on Viking and just outside the range based on Pathfinder. Using a Martian soil simulant that weighs the same in Earth's gravity as Martian soil weighs in Mars' gravity could allow researchers and engineers to develop vehicles and structures that are much better prepared to perform as intended on the surface of Mars. Fillite may also

have its benefits for lunar regolith simulation as well since many of its properties are similar to lunar regolith and its unit weight is much closer to lunar regolith than most lunar simulants currently in use.

3. The internal friction angle of Fillite compared well with that estimated by Pathfinder, but was considerably higher than what was calculated using the data from the Viking landers. Conversely, the cohesion of Fillite was found to be much closer to what was inferred by the Viking landers but was much higher than what was estimated with Pathfinder data. The discrepancies between Pathfinder and the Viking landers are most likely due to the fact that neither had the ability to directly measure these properties, but rather had to infer them from various images and other tests. Nonetheless, the strength properties of Fillite correspond to values estimated by at least one of the explorations of the lander.
4. The compression index of Fillite is lower than other lunar simulants but still falls within the range of lunar soil. The recompression index is larger than other simulants but is approximately equal to the largest value that was measured on lunar soil. No compression data are currently available on Martian soil, but it can be concluded that Fillite behaves similarly to lunar soil under one dimensional compression conditions.
5. The shear wave velocity of Fillite ranged from 126.6 m/s at the lowest density (~20%) and confining pressure (12.5 kPa) to 277.8 m/s at the highest density (~75%) and confining pressure (150 kPa). Using these results, the maximum shear modulus ranged from 6.9 to 39.5 MPa.

In summary, Fillite has many physical and mechanical properties that are similar to what is known about Martian regolith. Comparing properties of Fillite to lunar regolith when properties of Martian regolith are not well known still yields comparable results. Also, because Fillite is light-weight, readily available, chemically inert, and can be reused after anticipated applications related to rover mobility studies, it is a suitable simulant for rover mobility studies applicable to Mars and the Moon. Fillite is quite dilatant; its peak and critical angles of internal friction are smaller than those of most other simulants. Smaller shear strength, coupled with much smaller bulk unit weight as compared to other simulants, would result in smaller bearing and shearing resistances allowing for better simulation of the intended high-sinkage, high-slip situations for rover mobility studies.

Whenever possible, simple empirical correlations relating mechanical properties (elastic modulus, dilatancy angle, secant peak friction angle, small-strain shear wave velocity, and maximum shear modulus) of Fillite as a function of the state (relative density or void ratio) and confining pressure are provided so these properties can be readily estimated to support further analytical studies.

Acknowledgements

This work has been supported by the Vermont Space Grant under NASA Cooperative Agreement #NNX10AK67H. The authors are grateful to Mr. Colin Creager and Dr. Juan Agui of NASA Glenn Research Center for providing Fillite and general support for the study. The Authors are also thankful for Dr. Adam Sevi's assistance in conducting maximum and minimum density tests reported here.

References

Allen, C., Lindstrom, R., Lindstrom, M,, and Lockwood, J. (1997) "JSC MARS-1: MARTIAN REGOLITH SIMULANT." *Lunar and Planetary Science XXVIII*

Alshibli, K., and Hasan, A. (2009) "Strength Properties of JSC-1A Lunar Regolith Simulant." *Journal of Geotechnical and Geoenvironmental Engineering* 135.5: 673.

Alshibli, K., and Sture, S. (2000) "Shear Band Formation in Plane Strain Experiments of Sand." *Journal of Geotechnical and Geoenvironmental Engineering* 126.6: 495.

ASTM D2425 (1991) "Standard Test Methods for One-Dimensional Consolidation Properties of Soils Using Incremental Loading"

ASTM D854 (1991) "Standard Test Methods for Specific Gravity of Soils by Water Pyncnometer"

ASTM D4253 (2006) "Standard Test Methods for Maximum Index Density and Unit Weight of Soils Using a Vibratory Table."

ASTM D4254 (2006) (Standard Test Methods for Minimum Index Density and Unit Weight of Soils and Calculation of Relative Density)

ASTM D2850 (2007) "Standard Test Methods for Unconsolidated-Undrained Triaxial Compression Test for Cohesive Soils"

ASTM D6913 (2009) "Standard Test Methods for Particle-Size Distribution (Gradation) of Soils Using Sieve Analysis"

Blewett, J., Blewett, I.j., and Woodward, P.k. (2000) "Phase and Amplitude Responses Associated with the Measurement of Shear-wave Velocity in Sand by Bender Elements." *Canadian Geotechnical Journal* 37.6: 1348-357.

Bolton, M. D. (1986) "The Strength and Dilatancy of Sands." *Géotechnique* 36.1: 65-78.

Chaney, R., Demars, K., Brignoli, E., Gotti, M., and Stokoe, K. (1996) "Measurement of Shear Waves in Laboratory Specimens by Means of Piezoelectric Transducers." *Geotechnical Testing Journal* 19.4: 384.

Dyvik, R., and Madshus, C. (1985) "Lab Measurements of G_{max} Using Bender Elements." *Advances in the Art of Testing Soils under Cyclic Conditions: Proceedings of a Session*. By Vijay Khosla. New York, NY: American Society of Civil Engineers.

Edmunson, J. (2010) "Simulant Listing" *NASA - In Situ Resource Utilization*.

Fang, H.-Y. (1990), Foundation Engineering Handbook, 2nd ed., Kluwer Academic Publishers.

Hardin, B. O., and Richart, F. E. (1963) "Elastic Wave Velocities in Granular Soils." *Journal of Soil Mechanics and Foundations Division* 33.1: 33-65.

He, C., Zeng, X., and Wilkinson, A. (2011) "Geotechnical Properties of GRC-3 Lunar Simulant." *Journal of Aerospace Engineering* 26: 528-534

Heiken, G., Vaniman, D., and French, B. (1991) *Lunar Sourcebook: A User's Guide to the Moon*. Cambridge: Cambridge UP.

Kulhway, F.H. and Mayne, P.W. (1990) "Manual on Estimating Soil Properties for Foundation Design." *Report EPRI EL-6800,* Prepared for Electric Power Research Institute.

Lee, J-S., and Santamarina, J. (2005) "Bender Elements: Performance and Signal Interpretation." *Journal of Geotechnical and Geoenvironmental Engineering* 131.9: 1063.

Li, Y., Zeng, X., and Agui, J. (2013) "Developing a Light Weight Martian Soil Simulant (CWRU1) for High Sinkage Mobility Test." *Journal of Aerospace Engineering*: 130807091030006.

Moore, H. J., Clow, G. D., and Hutton, R. E. (1982) "A Summary of Viking Sample-Trench Analyses for Angles of Internal Friction and Cohesions." *Journal of Geophysical Research* 87.B12: 10043-0050.

Moore, H., and Jakosky, B. (1989) "Viking Landing Sites, Remote-sensing Observations, and Physical Properties of Martian Surface Materials." *Icarus* 81.1: 164-84.

Moore, H., Bickler, D., Crisp, J., Eisen, H., Gensler, J., Haldemann, A., Matijevic, J., Reid, L., and Pavlics, F. (1999) "Soil-like Deposits Observed by Sojourner, the Pathfinder Rover." *Journal of Geophysical Research* 104.E4: 8729-746.

NASA, (2009) "Spirit Rover Mission Update, Sol 1900-1906." http://mars.jpl.nasa.gov/mer/mission/status_spiritAll_2009.html#sol2100

Oravec, H. A., Zeng, X., and Asnani, V. M. (2010) "Design and Characterization of GRC-1: A Soil for Lunar Terramechanics Testing in Earth-ambient Conditions." *Journal of Terramechanics* 47.6: 361-77

Peters, G., Abbey, W., Bearman, G., Mungas, G., Smith, A., Anderson, R., Douglas, S. and Beegle, L. (2008) "Mojave Mars Simulant—Characterization of a New Geologic Mars Analog." *Icarus* 197.2: 470-79.

Seiferlin, K., Ehrenfreund, P., Garry, J., Gunderson, K., Hütter, E., Kargl, G., Maturilli, A., and Merrison, J. (2008) "Simulating Martian Regolith in the Laboratory." *Planetary and Space Science* 56.15: 2009-025.

Sirles, P. C., and Viksne, A. (1990) "Site-Specific Shear Wave Velocity Determinations for Geotechnical Engineering Applications". *Geotechnical and Environmental Geophysics, Investigations in Geophysics No. 5, Society of Exploration Geophysicists*, Tulsa, OK, pp 121-131.

Stoker, C.R., Gooding, J.L., and Roush, T. (1993) "The Physical and Chemical Properties and Resource Potential of Martian Surface Soils." *Resources of Near-Earth Space*. By Banin, A., D. Burt, and B.C. Clarke. Tucson: U of Arizona.

Sullivan, R., Anderson, R., Biesiadecki, J., Bond, T., and Stewart, H. (2011) "Cohesions, Friction Angles, and Other Physical Properties of Martian Regolith from Mars Exploration Rover Wheel Trenches and Wheel Scuffs." *Journal of Geophysical Research* 116.E2. DOI: 10.1029/2010JE003625

Tolsa USA Inc, http://www.thecarycompany.com/products/Tolsa/tolsa-usa-inc-fillite.html, last accessed: July 5,2014

Vermeer, P. A., and Schanz, T. (1996) "Angles of Friction and Dilatancy of Sand." *Géotechnique* 46.1: 145-51.

Viggiani, G., and Atkinson, J.h. (1995) "Stiffness of Fine-grained Soil at Very Small Strains." *Géotechnique* 45.2: 249-65.

Table 2.1: Properties of Fillite reported by the supplier (Tolsa USA Inc., 2014)

Particle size range	5 – 500 μm
Average bulk density	0.4 - 0.49 g/cc
Packing factor	60 - 65%
Hardness	Mohs Scale 6
Average wall thickness	5-10% of sphere diameter
Melting temperature	1400˚C (2550˚F)
Thermal conductivity	0.11 $Wm^{-1}k^{1}$
Loss on ignition	2% maximum
Surface moisture	0.3% maximum
Crush strength	13789.5 – 27579 kPa
Oil absorption	16 – 18 g oil/100 g

Table 2.2. Summary of laboratory tests conducted and their corresponding ASTM standards

Test	**ASTM Standard**	**Parameters Measured**
Mechanical sieve analysis	ASTM D6913 - Standard Test Methods for Particle-Size Distribution (Gradation) of Soils Using Sieve Analysis	Particle size distribution
Specific gravity test	ASTM D854 (Standard Test Methods for Specific Gravity of Soils by Water Pyncnometer)	Specific gravity (G_s)
Maximum and minimum bulk density	ASTM D4253 - Standard Test Methods for maximum Index Density and Unit Weight of Soils Using a Vibratory Table) and ASTM D4254 (Standard Test Methods for Minimum Index Density and Unit Weight of Soils and Calculation of Relative Density	Maximum and minimum dry densities (ρ_{max} and ρ_{min}, respectively)
Triaxial compression test	ASTM D2850 - Standard test Methods for Unconsolidated-Undrained Triaxial Compression Test for Cohesive Soils (modified as needed)	Peak and critical shear strength parameters (cohesion [c] and friction angle [ϕ])
One-dimensional compression test	ASTM D2435 - Standard Test Methods for One-Dimensional Consolidation Properties of Soils Using Incremental Loading (modified as needed)	Compression and recompression indices (c_c and c_r, respectively)
Bender element test	Not available	Shear wave velocity (V_s)

Table 2.3. Index properties of Fillite

Specific Gravity	0.669
Minimum Density (g/cc)	0.415
Maximum Density (g/cc)	0.476
Minimum Porosity	0.288
Maximum Porosity	0.379
Minimum Void Ratio	0.405
Maximum Void Ratio	0.610

Table 2.4. Mechanical properties of Fillite

Relative Density D_r (%)	Peak Shear Strength Mohr-Coulomb Parameters		Critical State Shear Strength Mohr-Coulomb Parameters		Confining Pressure σ_3 (kPa)	Secant Friction Angle		Dilatancy Angle ψ (deg)	Young's Modulus, E_{ur} (MPa)	Poisson's Ratio υ
	Cohesion c_p (kPa)	Friction Angle ϕ_p (deg)	Cohesion c_{cs} (kPa)	Friction Angle ϕ_{cs} (deg)		Peak	Critical State			
22.7	1.2	33.0°	0.4	32.9°	25	34.2	33.2	10.7	19.6	0.32
					50	33.8	33.0	10.0	26.5	0.34
					100	33.4	32.6	8.8	36.7	0.37
					150	33.0	32	7.05	49.5	0.39
39.3	4.6	34.2°	2.4	32.7°	25	36.8	35.3	15.1	27.2	0.40
					50	35.7	34.5	12.3	34.3	0.34
					100	35.1	33.6	11.0	48.2	0.32
					150	35.0	33.2	9.1	64.0	0.38
63.6	3.6	34.6°	2.1	33.1°	25	36.6	34.4	19.8	31.7	0.30
					50	35.7	33.7	17.7	40.9	0.32
					100	35.1	33.4	14.9	55.2	0.41
					150	35.0	33.5	11.3	71.9	0.38
74.5	2.9	37.3°	0	36.4°	25	38.8	37.6	24.5	37.4	0.31
					50	36.0	36.4	20.5	44.2	0.32
					100	37.6	36.2	17.8	62.1	0.36
					150	37.5	36.5	13.4	73.2	0.38

Table 2.5. Shear wave velocities and maximum shear modulus values for Fillite.

Relative Density, D_r (%)	Confining Pressure	Shear Wave Velocity V_s (m/s)	Maximum Shear Modulus G_{max} (MPa)	K_{2max}
24.0	12.5	126.6	6.9	10.2
	25	166.8	11.9	
	50	194.6	16.2	
	75	217.0	20.2	
	100	228.3	22.3	
	150	248.8	26.5	
40.5	12.5	150.1	9.9	11.5
	25	176.3	13.6	
	50	203.8	18.2	
	75	220.5	21.3	
	100	231.0	23.4	
	150	247.9	26.9	
62.0	12.5	148.7	10.0	12.5
	25	179.6	14.5	
	50	218.5	21.5	
	75	222.9	22.3	
	100	236.8	25.3	
	150	258.6	30.2	
76.0	12.5	145.1	9.7	13.9
	25	192.7	17.1	
	50	217.0	21.7	
	75	242.6	27.1	
	100	255.3	30.0	
	150	277.8	35.5	

Table 2.6. Index and Strength Property comparison of Fillite to Martian and Lunar soils and simulants ([1]Moore et al, 1999; [2]Moore, Clow, and Huttom 1982; [3]Peters et al., 2008; [4]Allen et al., 1998; [5]Li et al., 2013; [6]Heiken 1991; [7]Oravec, 2009; [8]Alshibli and Hasan 2009)

Soil Properties	Fillite	Martian Soil		Martian Simulants			Lunar Soil[6]	Lunar Simulants	
		Pathfinder[1]	Viking 1 & 2[2]	MMS Dust[3]	JSC-Mars 1[4]	CWRU-1[5]		GRC-1[7]	JSC-1A[8]
Median Particle Size, D_{50} (mm)	0.18	-	-	0.2	0.41	0.7	0.04-.13	0.27	0.1
D_{10} (mm)	0.13	-	-	0.002	0.15	0.19	0.013	0.094	0.017
D_{30} (mm)	0.2	-	-	0.0145	0.24	0.503	0.034	0.160	0.042
D_{60} (mm)	0.21	-	-	0.035	0.61	1.22	0.14	0.39	0.11
Coefficient of Uniformity, C_u	1.62	-	-	17.5	4.07	6.42	10.769	4.15	6.47
Coefficient of Curvature, C_c	1.47	-	-	3	0.63	1.09	0.635	0.698	0.94
Maximum Bulk Density, ρ_{max} (kg/m^3)	476.1	1518	1300	-	1115	916	1810	1890	2028
Minimum Bulk Density, ρ_{min} (kg/m^3)	415.4	1285	1000	-	885	621	920	1600	1566
Specific Gravity, G_s	0.669	-	-	-	1.91	1.51	2.3-3.2	2.58	2.875
Bulk Unit Weight (kN/m^3), Υ	4.07-4.67	4.77-5.63	3.71-4.82	-	8.67-10.93	6.09-8.98	1.49-2.94	15.68-18.52	15.35-19.87
Maximum Void Ratio, e_{max}	0.61	-	-	-	1.16	0.65	1.8	0.613	0.826
Minimum Void Ratio, e_{min}	0.405	-	-	-	0.71	1.43	0.712	0.364	0.41
Maximum Porosity, n_{max}	0.379	-	-	-	0.54	0.59	0.97	0.380	0.452
Minimum Porosity, n_{min}	0.288	-	-	-	0.42	0.39	0.416	0.267	0.29
Compression Index, c_c	0.041	-	-	-	-	0.137-0.345	0.012-0.108	0.03	0.068
Recompression Index, c_r	0.014	-	-	-	-	0.008-0.012	0-0.013	0.008	0.001
Peak Friction Angle, ϕ_p (deg)	33.0-37.3	15.1-33.1	15.6-20.4	30-31	47	30.6-39.9	30-50	29.8-44.4	41.9-56.7
Peak Cohesion, c_p (kPa)	1.2-4.6	0.18-0.57	0.4-2.8	0.38-0.53	1.91	5-11	0.4	0-9.92	3.5
Critical Friction Angle, ϕ_{cs} (deg)	32.9-36.4	-	-	-	-	-	-	-	35.5-51.0
Critical Cohesion, c_{cs} (kPa)	0-2.4	-	-	-	-	-	-	-	-
Dilatancy Angle, ψ (deg)	7.1-24.5	-	-	-	-	-	-	-	2.6-25.8
Young's Modulus, E_{ur} (MPa)	19.6-73.2	-	-	-	-	-	-	-	10.3 - 80
Poisson's Ratio, υ	0.3-0.41	-	-	-	-	-	-	-	0.4 – 0.47
Small-strain Shear Wave Velocity, v_s (m/s)	126.6-277.8	-	-	-	-	-	40-400	-	-
Small-strain Shear Modulus, G_{max} (MPa)	6.9-35.5	-	-	-	-	-	1.47-289.6	-	-

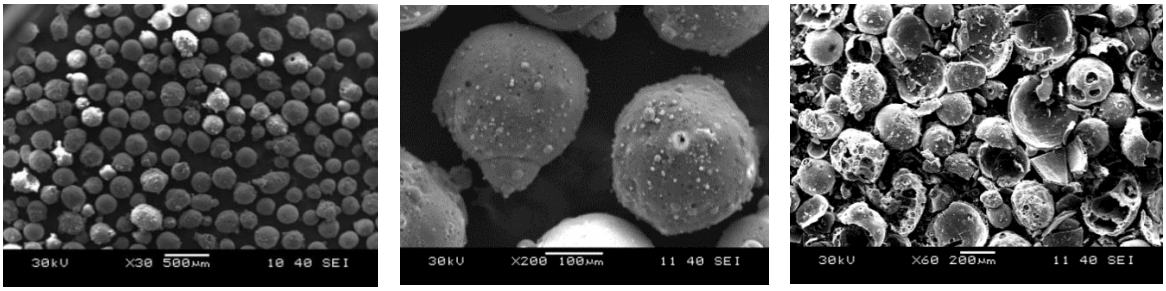

a) 30x magnification

b) 200x magnification

c) Intentionally broken particles under 60x magnification

Figure 2.1. Images of Fillite particles taken using a scanning electron microscope.

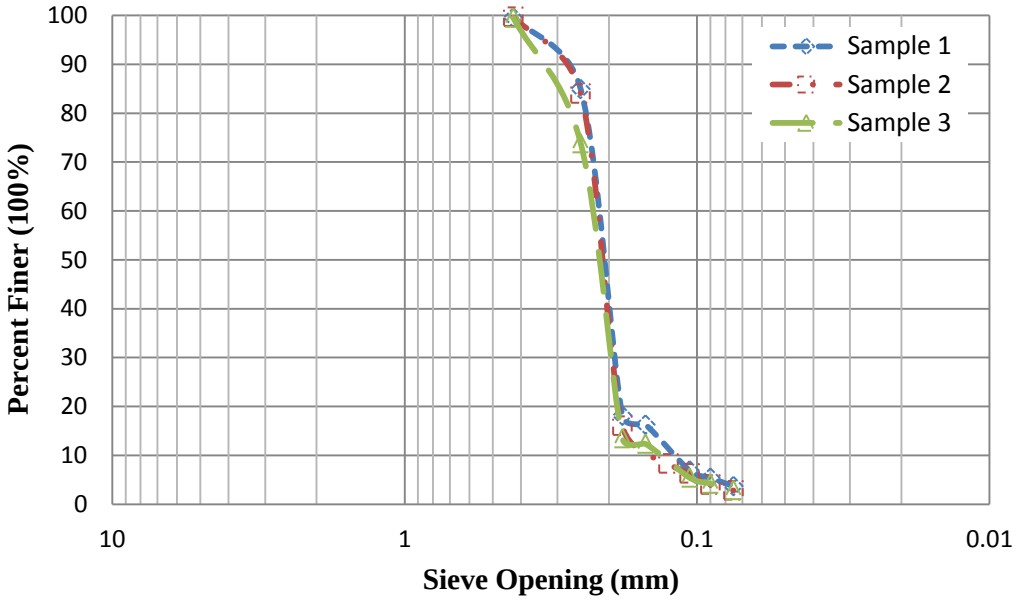

Figure 2.2. Grain size distribution analysis results of three separate random samples of Fillite.

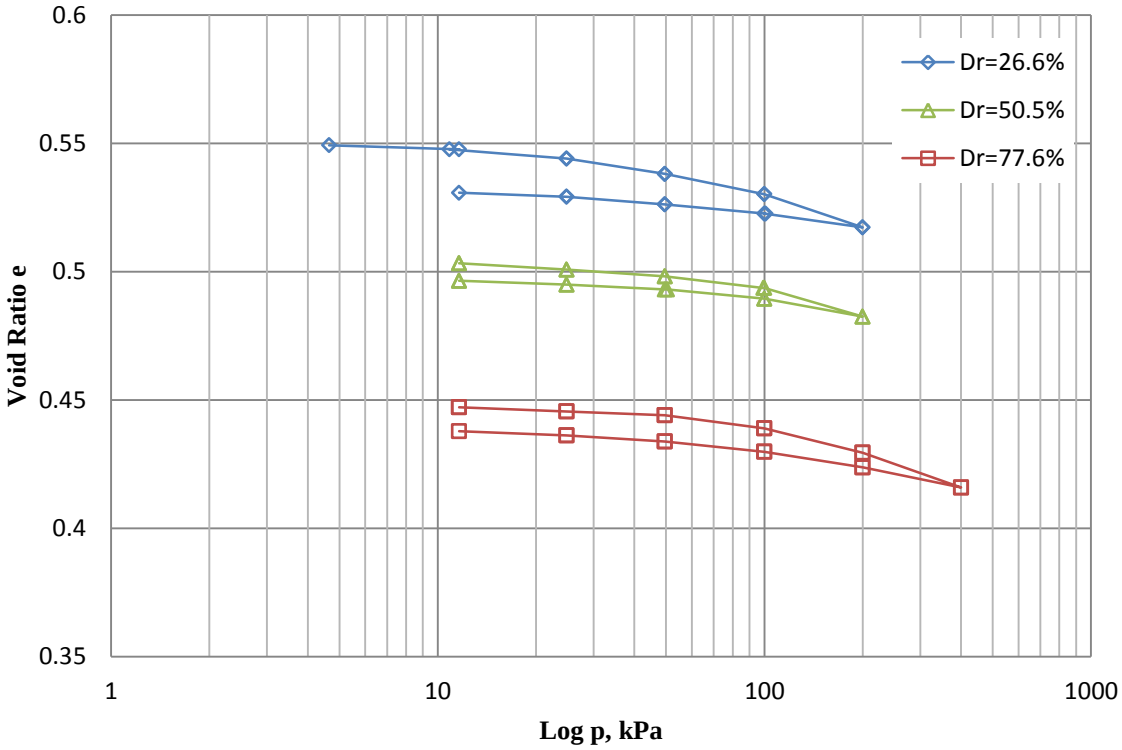

Figure 2.3. Compression curves for Fillite at three relative densities.

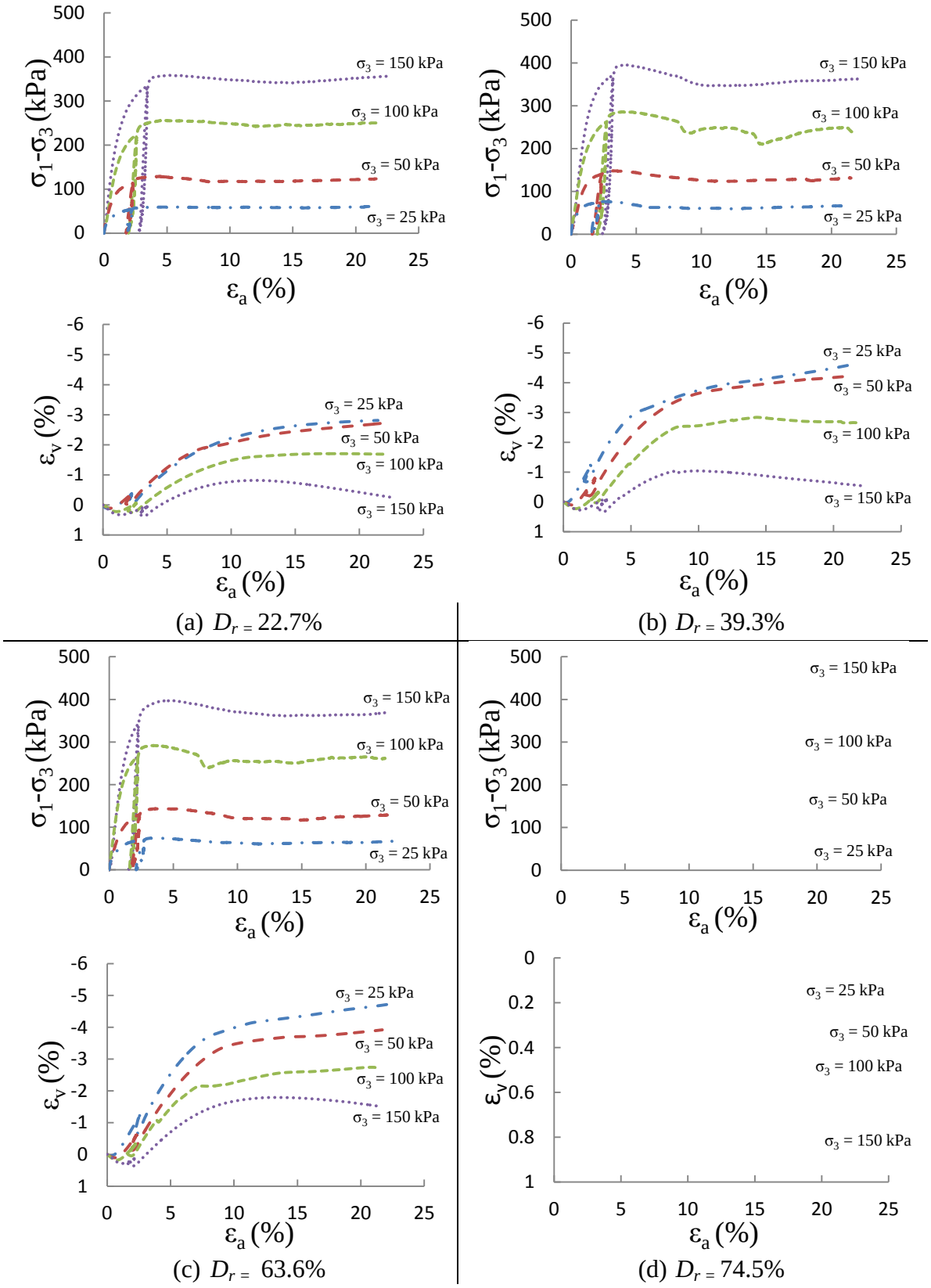

Figure 2.4: Results of the triaxial test series on Fillite

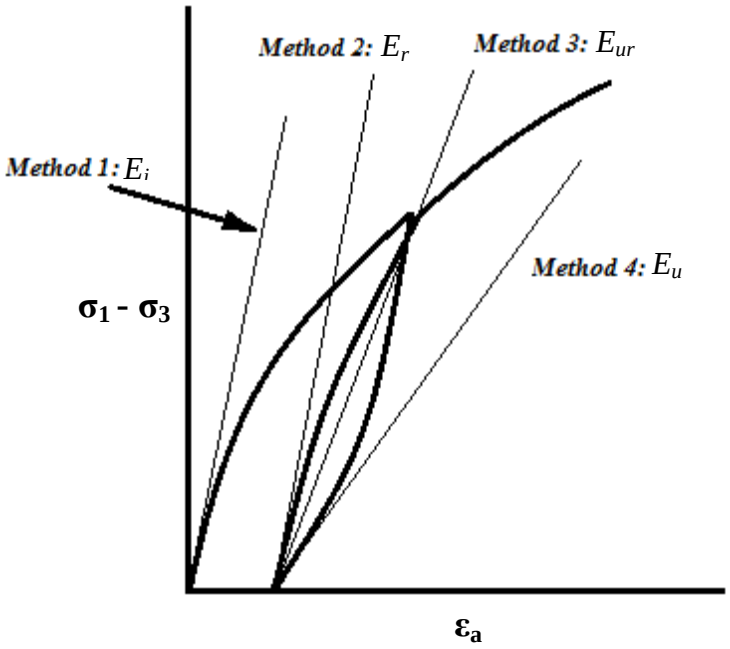

Figure 2.5: Different methods to calculate Young's elastic modulus; method 3 was used in this work.

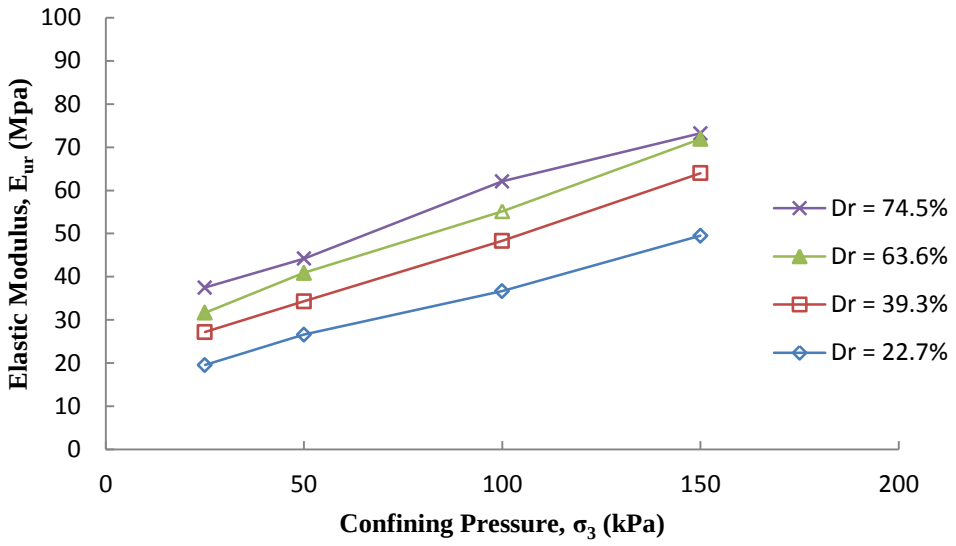

a) Measured elastic modulus variation with confining pressure.

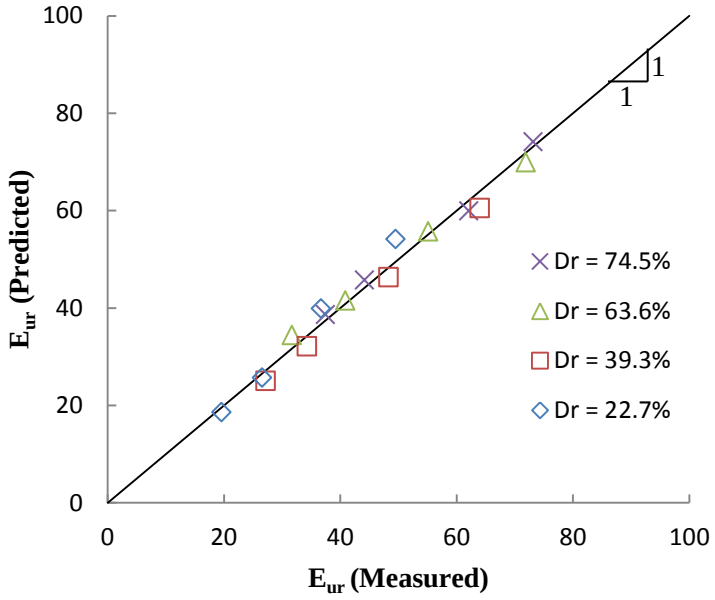

b) Measured versus predicted elastic modulus.

Figure 2.6. Variation of measured elastic modulus as a function of confining pressure and relative density and its comparison to predicted modulus per equation 6.

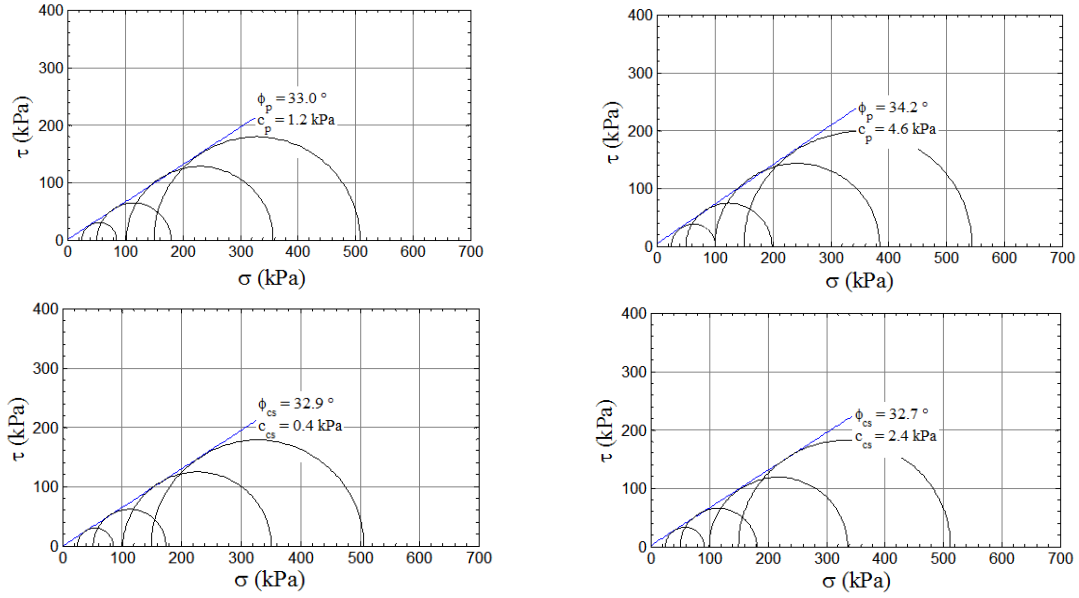

a) D_r = 22.7%

b) D_r = 39.3%

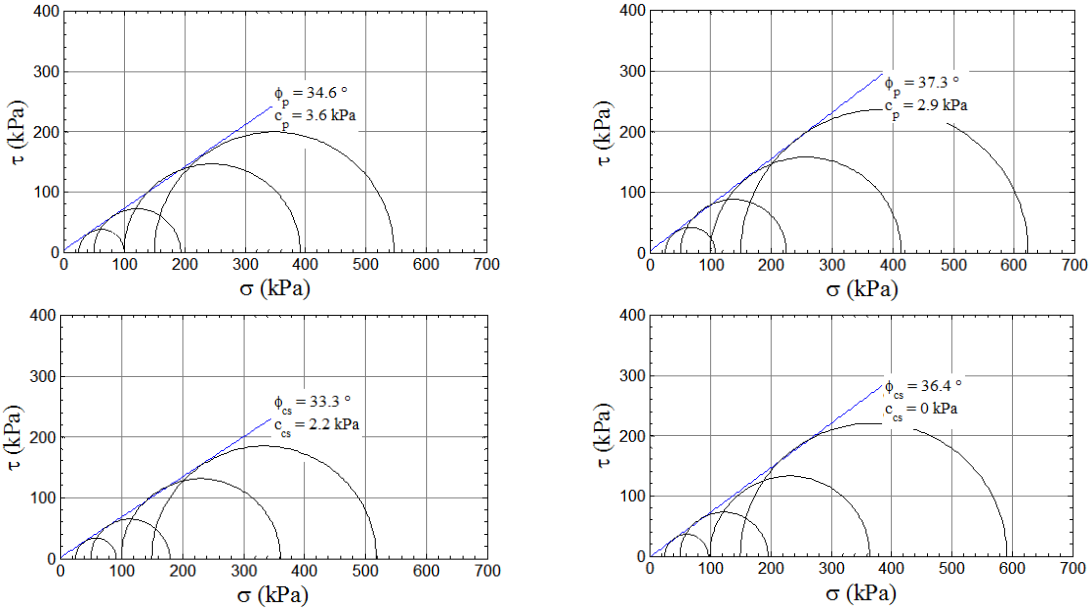

c) D_r = 63.6%

d) D_r = 74.5%

Figure 2.7. Mohr-Coulomb failure envelopes for Fillite for peak state stress (top) and critical state stress (bottom).

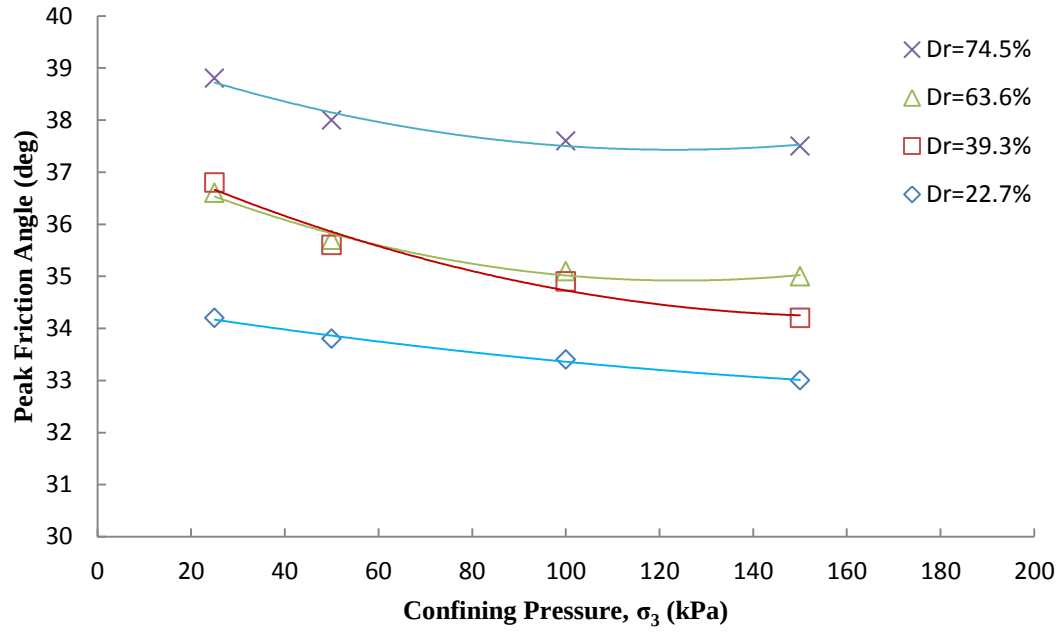

a) Secant peak friction angle as a function of confining pressure.

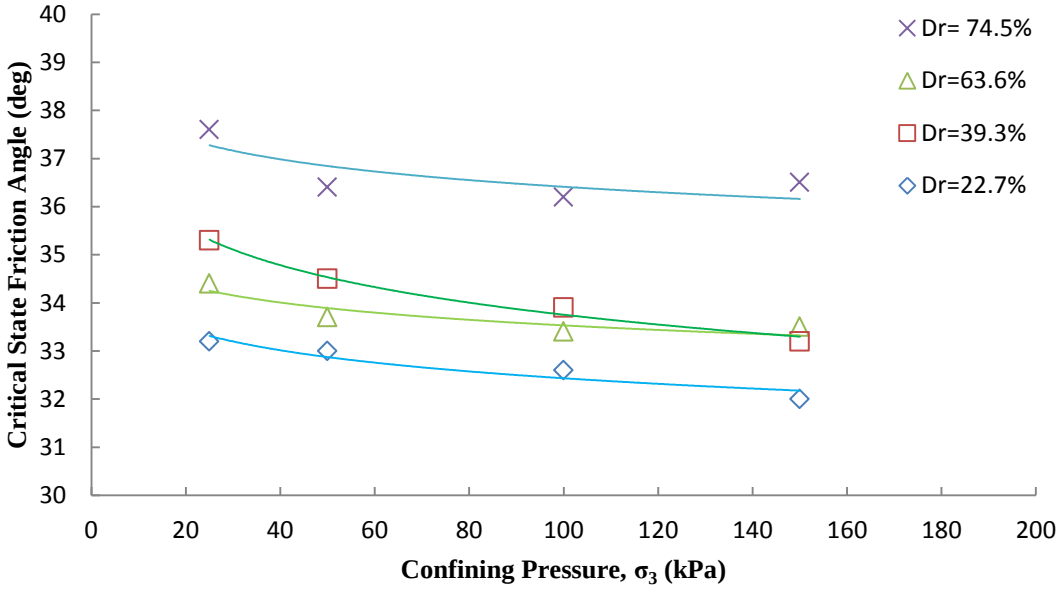

b) Secant critical friction angle as a function of confining pressure.

Figure 2.8. Secant peak and critical friction angles of Fillite as a function of confining pressure and relative density.

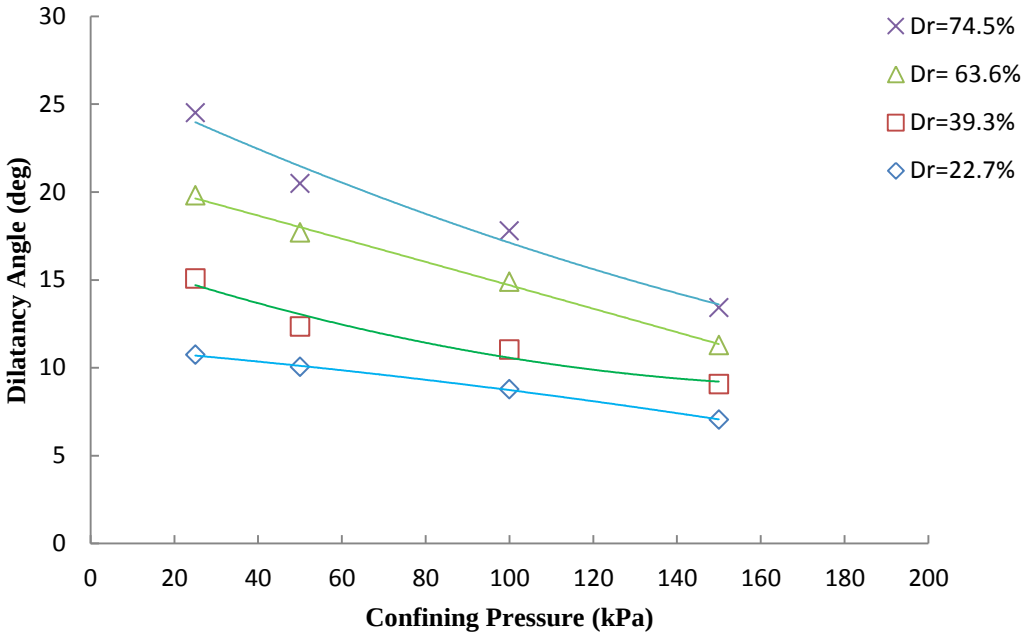

Figure 2.9. Variation of dilatancy angle as a function of confining pressure and relative density of Fillite.

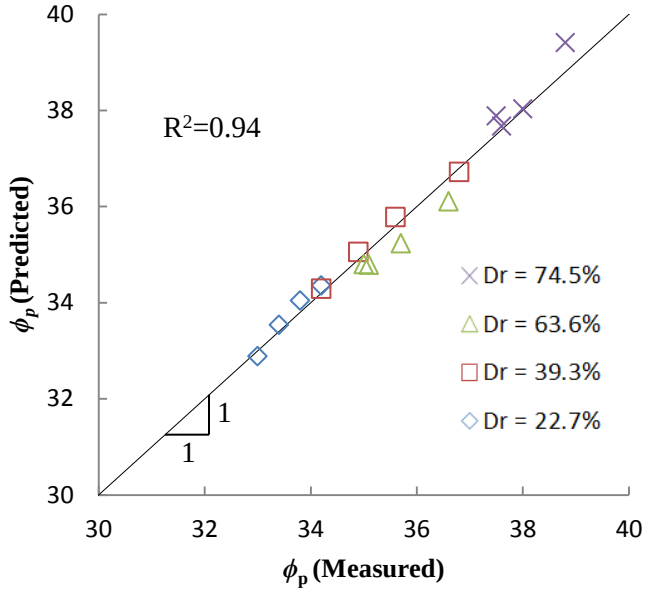

a) Measured versus predicted secant peak friction angle.

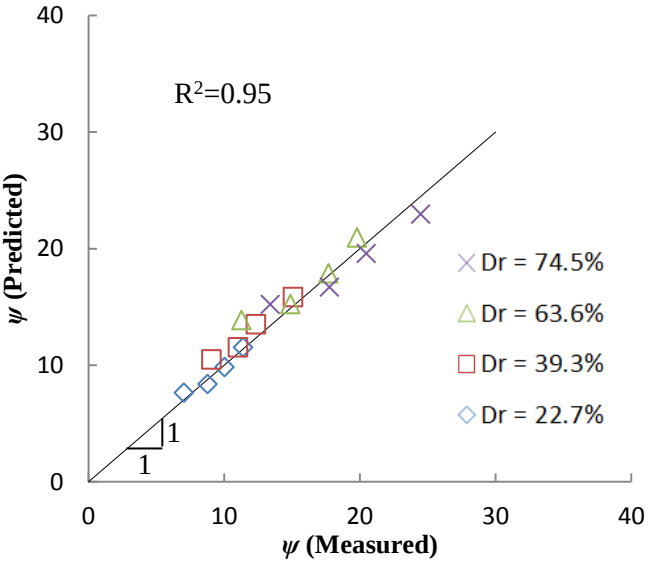

b) Measured versus predicted dilatancy angle.

Figure 2.10. Measured versus predicted (per equations 13a and 13b) secant peak friction angle and dilatancy angle.

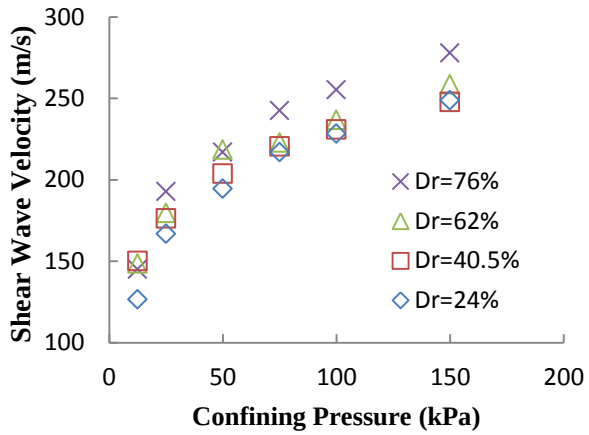

(a) Measured shear wave velocity.

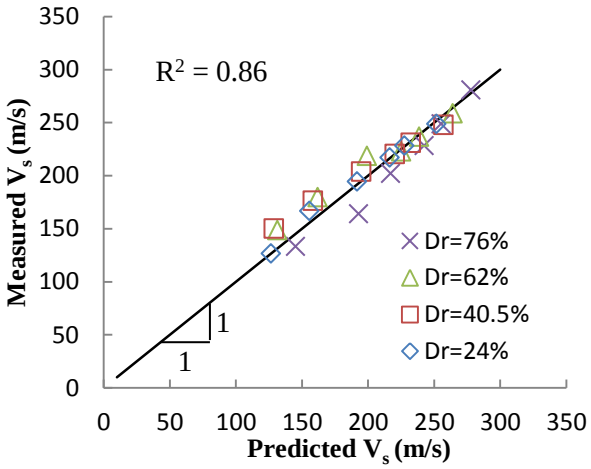

(b) Measured versus predicted (Hardin and Richart 1963) shear wave velocity.

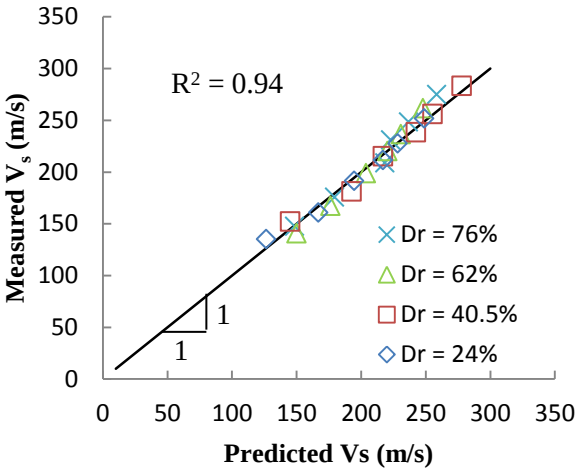

(c) Measured versus predicted (proposed equation 16) shear wave velocity.

Figure 2.11. Measured shear wave velocities and their predictions per equation 15 (Hardin and Richart 1963) and proposed equation 16.

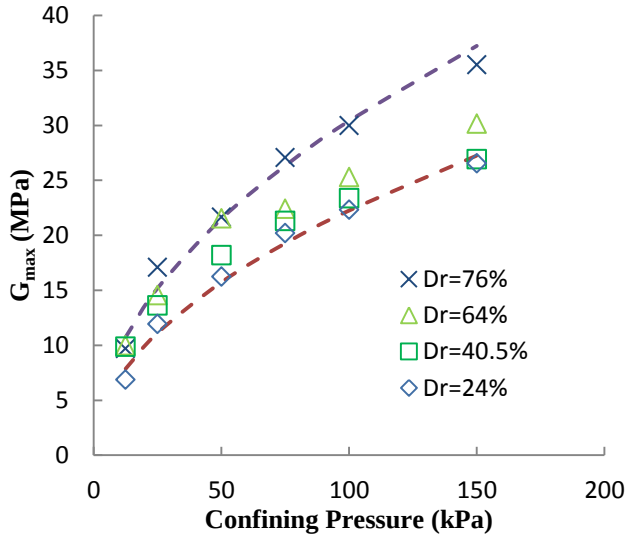

(a) Measured maximum shear modulus.

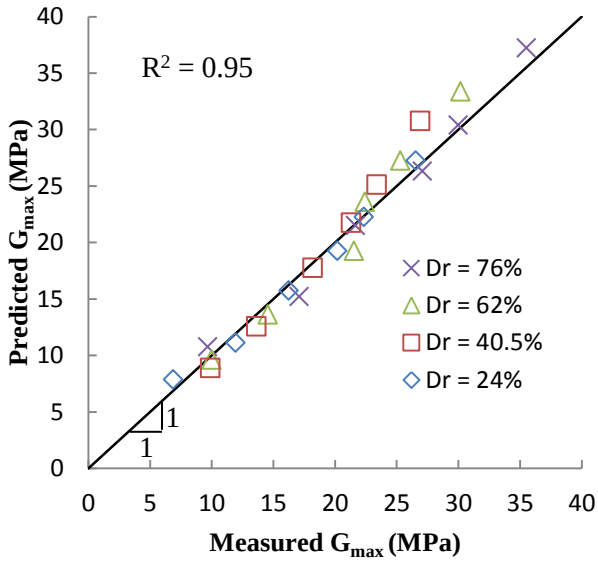

(b) Measured and predicted maximum shear modulus per equation 18.

Figure 2.12. Measured G_{max} with the Seed and Idriss (1970) prediction model for upper and lower bounds and comparison of measured G_{max} and predicted G_{max}.

CHAPTER 3: PRESSURE SINKAGE MODELING OF FILLITE FOR PLANETARY ROVER MOBILITY APPLICATIONS

3.1 Abstract

This paper presents an investigation examining pressure-sinkage behavior of a light-weight, granular material called Fillite in support of modeling rover mobility in high-sinkage, high-slip environments found on Mars, the Moon, and other planetary bodies. Fillite is composed of alumino-silicate hollow microspheres and is harvested from the pulverized fuel ash of coal-fired power plants. It is a light, granular material that is also chemically inert and available in large quantities for laboratory studies. A bevameter apparatus at National Aeronautics and Space Administration (NASA) Glenn Research Center was used to perform normal sinkage tests on Fillite to obtain pressure sinkage-curves at three different densities and three different plate diameters. The test results were used to determine parameters for both the Bekker model and the New Model of Mobility (N2M) sinkage model. These parameters were then used to predict the sinkage of a Spirit rover wheel if the rover were to be used on Fillite. The predicted sinkage of a Spirit rover wheel in Fillite was 84% of the wheel diameter, which was within the observed sinkage of 50 to 90% of the wheel diameter of the Spirit rover on Mars. Shear bevameter tests were also performed on Fillite to assess the shear stresses and shear deformations imparted by wheels under torsional loads. The results compared well to the estimated shear stresses and deformations of Martian soil caused by the wheels of the Spirit rover. When compared to other simulants (e.g. GRC-1), the pressure-sinkage and shear stress-shear deformation behaviors of Fillite confirm that Fillite is more suitable for high-

sinkage and high-slip rover studies than other typical simulants derived from natural terrestrial soils and rocks.

3.2. Introduction

Generally, the performance of any prototype or model rover that is to be sent to another planet or the Moon is evaluated in test beds that typically use simulants derived from terrestrial soils. Examples of such simulants for rover testing are GRC-1 lunar strength simulant (Oravec, 2009), JSC-1 lunar simulant (Alshibli and Hasan, 2009), and MMS Martian simulant (Peters et al, 2008). While these simulants may mimic the average terrain response on the Moon or Mars under a roving vehicle, there are situations where high-sinkage/high-slip environments can be encountered. In general, pockets of fine, low strength sand-like material are fairly uncommon on Mars because its surface is mostly a combination of fine dust, loose clods, and larger rocks (Moore, 1982). However, the areas of high-sinkage soil, when present can produce significant challenges for rovers and the standard simulants listed above are typically unable to replicate these challenges. An example of such a situation resulted in the Spirit Rover becoming permanently entrenched on Mars in May 2009 (McKee, 2009). This event helped to provide the motivation to select a Martian regolith-like material that behaves not only similar to the loose drift Martian soil that is present on the Mars' surface, but in general exhibits higher sinkage behavior than current terrestrial soil simulants. NASA Glenn Research Center has selected a light-weight, granular material called Fillite for their test bed in a "sink tank", for use in rover mobility studies. Suitability of Fillite as a high-sinkage, high-slip material for rover studies is examined in this paper. For this purpose, normal and shear

bevameter tests were conducted on Fillite. The bevameter test results were used to obtain parameters of select models available in the literature.

The bevameter test was developed by Bekker (1956) specifically to evaluate the forces experienced by a wheel under typical loading conditions. Two types of bevameter tests are often conducted – normal test and shear test. To assess the response of a wheel to a normal load, a normal load-penetration bevameter test is conducted using a flat plate, a piston, a load cell and a displacement transducer. Because typically only the very bottom of a wheel is in contact with the ground, Bekker (1956) approximated that contact area to be flat and used the flat plates to evaluate the pressure and resistance forces experienced on that surface. The piston presses the plate into the soil specimen and the corresponding load and vertical displacement of the plate are recorded to obtain the pressure-sinkage relationship of the soil.

During a shear bevameter test, an annular shear ring under a preselected normal stress is used to simulate shearing action of the vehicle running-gear by rotating on the terrain surface. The applied torque and corresponding angular displacement are measured during the test.

There have been several pressure sinkage models developed over the years, the first of which is the Bernstein – Goriatchkin model (1937). This model gave rise to the Bekker model (1969), which is the most common pressure-sinkage model in use. This model is evaluated later in the paper using the results of normal bevameter tests. Gotteland and Benoit (2006) developed a model called the New Model of Mobility (N2M), which is also assessed here. These two models were selected because parameters for both models can be determined using the same test results. A third model, known as

the Bekker-Wong model (Wong, 2010), is also presented later. The Bekker model and N2M sinkage model are first briefly described below.

3.2.1 Bekker Model

Bernstein-Goriatchkin model (1937) suggested the following experimentally-determined pressure-sinkage relationship:

$$p \cong k\, z^{0.5} \tag{1}$$

where z is the penetration depth of the plate subjected to a normal pressure p, k is a modulus of inelastic deformation, and 0.5 is the exponent of sinkage (Oravec, 2009). It was later argued that the exponent of 0.5 in equation1 should be replaced with "n", which ranges between zero and one (Bekker, 1969; Goriatchkin et al., 1936; Oravec, 2009). In general, the above pressure-sinkage equations were found to be very limited in application as the value of k depended on the size and shape of the test plate, and therefore, not a true modulus of deformation (Oravec, 2009).

The Bekker pressure-sinkage model appears to be one of the most widely used models for predicting the pressure-sinkage behavior of a homogenous soil. Bekker (1969) developed his model by modifying the above Bernstein-Goriatchkin model (1937) and was written as:

$$p = \left(\frac{k_c}{b} + k_\phi\right) z^n \tag{2}$$

where p is the pressure, z is the sinkage as before, b is the smaller dimension of the rectangular plate or the diameter of a circular plate, and k_c and k_ϕ are moduli of deformation with respect to cohesion and friction, respectively, and n is the empirical soil value which defines the shape of the load-penetration curve. The units for k_c and k_ϕ are

p/L^{n-1} and p/L^n, respectively, where p is the pressure and L is length. Bekker was able to show that the stiffness coefficients are independent of plate geometry in homogenous terrain (Bekker, 1969). Oravec (2009) noted that equation 2 is basically a generalized form of the well-known load-penetration equation for structures in civil engineering, where n is equal to one and b is equal to the depth of the structure (Taylor, 1948).

In order to determine the values of k_c, k_ϕ, and n, a minimum of two pressure sinkage tests are needed with two different plate sizes. The two curves produced from these tests can be approximated as:

$$p_1 = \left(\frac{k_c}{b_1} + k_\phi\right) z^n \tag{3}$$

$$p_2 = \left(\frac{k_c}{b_2} + k_\phi\right) z^n \tag{4}$$

Taking the values of pressure where z = 1 on both curves gives two values of pressure, labeled as a_1 and a_2.

$$(p_1)_{z=1} = a_1 \tag{5}$$

$$(p_2)_{z=1} = a_2 \tag{6}$$

Two equations are available to determine k_c and k_φ, using the measured values above and the two known plate diameters. They are:

$$k_c = \frac{(a_1 - a_2) b_1 b_2}{(b_2 - b_1)} \tag{7}$$

$$k_\varphi = \frac{a_2 b_2 - a_1 b_1}{(b_2 - b_1)} \tag{8}$$

In order to find the last unknown coefficient n, it is helpful to express the two test curves in logarithmic form. They become:

$$\log p_1 = \log\left(\frac{k_c}{b_1} + k_\varphi\right) + n \log z \tag{9}$$

$$\log p_2 = \log\left(\frac{k_c}{b_2} + k_\varphi\right) + n \log z \tag{10}$$

Solving for n in both of the above equations produces a sinkage exponent for each individual plate. Averaging these exponents can produce a single exponent for the model.

3.2.2 N2M Sinkage Model

One of the more recent soil sinkage models is known as the New Model for Mobility, or N2M for short (Gotteland and Benoit, 2006). The goal for the model was to predict the pressure-sinkage relationship of a soil by assuming small vertical sinkages to be analogous to elastic soil behavior and large sinkages to be analogous to plastic soil behavior (Gotteland and Benoit, 2006). The N2M model equation stated below links experimentally observed linear behavior for small sinkages to the linear behavior for large sinkages by an exponential function.

$$p = \left(\frac{C_m}{b^m} + \frac{S_m}{b^{1-m}} z\right)\left(1 - exp\left\{-\frac{s_0}{C_m}\frac{z}{b^{1-m}}\right\}\right) \tag{11}$$

Much like the Bekker model, a minimum of two sinkage tests are needed to determine the four parameters m, C_m, s_m, and s_0 with two different plates used for each test. The parameter s_0 characterizes the elastic phase of the pressure-sinkage response and parameters C_m and s_m characterize the plastic phase of the pressure-sinkage response (Gotteland and Benoit, 2006). In order to calculate the exponent m, two graphical parameters need to be found:

$$A_m = \frac{s_m}{b^{1-m}} \tag{12}$$

$$A_0 = \frac{C_m}{b^m} \tag{13}$$

As shown in Figure 1a, A_m is the slope of the plastic region of the pressure-sinkage curve with units of p/L and A_0 is the projected y-intercept of the slope of the curve in the plastic region with units of p. The exponent m can then be calculated using the equation:

$$m = \frac{\ln B_2 A_{m,B_2} - \ln B_1 A_{m,B_1}}{\ln B_1 - \ln B_2} \tag{14}$$

The parameters of C_m and s_m can then be found by rearranging the equations for A_m and A_0. C_m has units of pL^m and s_m has units of pL^{-m}. This will give separate values for each individual test, so the parameters are typically averaged to produce a single set of values for the predictive model. The last parameter, s_0, can be found graphically by plotting the pressure-sinkage curve with the sinkage axis normalized by the plate diameter. The initial tangent of this pressure-sinkage curve equals s_0 and has units of p as depicted in Figure 1b.

3.3. Fillite

Fillite (Tolsa USA Inc., 2014) is composed of alumino-silicate hollow microspheres and is harvested from the pulverized fuel ash of coal-fired power plants. It is a light, granular material that is also chemically inert, free flowing and with strong particles (Tolsa USA Inc., 2014). Fillite is appears in several industrial applications that mix it into cement or an epoxy resin to provide both strength and a reduction in weight. Fillite (grade 500W-LF, off-white in color) used in this investigation and also used in the sink tank at NASA Glenn Research Center was obtained from Tolsa USA Inc. According to the supplier (Tolsa USA Inc., 2014), this Fillite has 34 - 40% alumina (as Al_2O_3), 55 – 65% of silica (as SiO_2) and maximum of 2% iron (as Fe_2O_3). In comparison to typical granular soils, the bulk density of Fillite is much lower with a range of 0.415 to 0.476

g/cm^3 (Edwards et al., in review). This gives Fillite a unit weight (on Earth) of about 4.0 to 4.7 kN/m^3, which is similar to that of Martian regolith (about 3.7 – 5.6 kN/m^3; the gravitational acceleration on Mars is 3.722 m/s^2 as opposed to 9.807 m/s^2 on Earth) and closer to the unit weight of lunar regolith (about 1.4 – 2.9 kN/m^3; the gravitational acceleration on the Moon is 1.6 m/s^2). It is important to match the unit weight of a simulant to that of the target soil/regolith, so the shear strength and sinkage properties are modeled correctly in the physical models. For example, Bin et al (2009) modeled pressure-sinkage data between a rigid wheel and a soil using the Distinct Element Method. They found that the computed sinkage considering the lunar gravity in the simulation was 22.5% to 57.6% greater than that when Earth's gravity was used under the same pressure condition.

An extensive material characterization of Fillite was undertaken to determine its geotechnical properties (Edwards, et al., in review). Grain size analysis revealed that 98% of Fillite particles were larger than 0.075 mm and smaller than 0.42 mm, with a mean particle size of about 0.2 mm. Fillite particles are quite uniform in size and spherical as seen in Figure 2. Per the Unified Soil Classification System (USCS), Fillite would classify as "poorly graded sand (SP)". The specific gravity of Fillite was determined to be 0.67. A series of triaxial compression tests and bender element tests on Fillite were also conducted by Edwards et al. (in review) at four densities (ranging from about 20% to 75% relative density) and four confining pressures (25, 50, 100 and 150 kPa). Each triaxial test included an unloading-reloading cycle. Based on these tests, the Young's modulus (unloading-reloading, E_{ur}) of Fillite ranged from 20 to 73 MPa, and the Poisson's ratio ranged from 0.3 to 0.41. These values are similar to those for typical

sands with Young's modulus ranging from 10 to 80 MPa and Poisson's ratio ranging from 0.20 to 0.45 (Kezdi 1974).The cohesion of Fillite was found to range from 0 to 4.6 kPa and the internal friction angles ranged between 32.9^{o} and 37.3^{o}. The dilatancy angle ranged from 7.1 to 24.5°. A series of bender element tests were also conducted to determine the small-strain shear wave velocity (v_s) of Fillite (Edwards et al, in review). The maximum shear modulus (G_{max}) could then be determined as $G_{max}=\rho v_s^2$ where ρ is the bulk density. The shear wave velocity of Fillite ranged from 126.6 m/s to 277.8 m/s. From these values, the calculated maximum shear moduli of Fillite ranged from 6.9 to 35.5 MPa. The compression and recompression indices of Fillite were also determined to be 0.041 and 0.014, respectively, using one-dimensional compression tests (Edwards, et al., in review). The compression and recompression indices of Fillite were determined to be 0.041 and 0.014, respectively. While no compression properties are known about Martian soil, these values are close to what has been determined for lunar regolith (Heiken et al, 1991). Table 1 provides a comparison of the properties of Fillite to the known or estimated properties of Martian and lunar regoliths. More detailed comparisons of material properties, including with select simulants, are summarized by Edwards, et al. (in review).

Fillite is quite dilatant, and its peak and critical angles of internal friction are smaller than those of most other simulants. Smaller shear strength, coupled with much smaller bulk unit weight as compared to other simulants, is expected to result in smaller bearing and shearing resistances allowing for better simulation of the intended high-sinkage, high-slip behavior for rover mobility studies.

3.4. Normal Bevameter Testing

This study used the bevameter available at the NASA Glenn Research. This setup had the capability to perform two types of bevameter tests typically used to evaluate soil-wheel interactions: a normal test and a shear test. To conduct a normal test, the machine utilized a piston for pressing a plate down into the soil specimen, a load cell for measuring the force of resistance, and laser range finders for continuously measuring the distance traveled (displacement). The shear test used the same components but with the addition of torque and angular motion sensors to measure the resistance to rotation as a constant normal load is being applied. In this section, results from the normal bevameter tests are presented.

3.4.1 Normal Bevameter Tests and Results

A photograph of the normal bevameter test setup appears in Figure 3. A circular test bin of 92 cm in diameter was filled to a depth of roughly 22.5 cm for each test. Fillite test beds were prepared at three relative densities of about 37, 55, and 77.5% in order to observe the pressure sinkage behavior for a wide range of possible sinkage conditions. While it was desired to use lower densities of Fillite, closer to 20%, it compressed quite significantly under its own weight. The lowest density that was consistently repeatable was 37%. It was also difficult to prepare uniform specimens at relative densities in excess of about 77.5%. Fillite was deposited into the bin using a hopper with a long tube. The Fillite was then gently and uniformly compressed with a large tamper as needed to reach higher densities for the desired tests. The depth of Fillite was measured in three locations

before each test was conducted. The average of these values was taken as the recorded depth for each test.

A minimum of two normal loads with two different plate sizes are needed to determine the sinkage constants for both prediction models. In this study, three different plate sizes were used, based on two criteria. The first is to satisfy the concept known as the "rule of five", which was proposed by Bekker (1969). The "rule of five" suggests that the diameter of the test bin should be at least five times that of the test plate to avoid sidewall boundary conditions. Bekker (1969) also suggested that the depth of the soil specimen should be approximately five times the intended sinkage to avoid bottom boundary effects. The second criterion was to match the effective contact area of past rover wheels. The effective contact area of a wheel is defined as the flat surface approximation of the portion of the wheel that has sunk into the soil. The wheel geometries of Sojourner, Spirit, and Curiosity Rovers were used to estimate the contact area. The contact surface for each wheel was estimated such that the length of the contact patch along the wheel was equal to one wheel radius. This resulted in an area of 0.0041 m^2 for the Sojourner wheel, 0.0173 m^2 for the Spirit wheel, and 0.0901 m^2 for the Curiosity wheel (Lindemann 2011). To that end, plate diameters of 7.6, 12.6, and 20.1 cm were used, each having a contact area of 0.0045 m^2, 0.0125 m^2, and 0.0317 m^2, respectively. While the largest plate area is less than the estimated Curiosity wheel contact area, it was the largest plate that could be used while holding closely to the rule of five with respect to the diameter of the bin holding the specimen. The bin diameter to plate diameter ratio of the 20.1 cm plate is just under 5 at 4.6. The plate was still used to observe the pressure sinkage behavior that Fillite may exhibit on larger contact surfaces.

Each plate was pushed into the bin under displacement control at a constant rate of 1 mm/min. Each test was performed at least twice to ensure repeatability.

A typical pressure-sinkage curve can be grouped into three zones, which are related to concepts in classical soil mechanics (Gotteland and Benoit, 2005). The first phase of the curve is a linear region, which is considered to be an elastic zone for small sinkage. This phase is followed by a transition period which asymptotes to a second linear region which can be equated to soil plasticity (Gotteland and Benoit, 2005). Figure 4 illustrates these zones.

The results of the normal bevameter tests are grouped by relative density and presented in Figure 5. The pressure-sinkage curves from the 7.6 cm plate and the 12.6 cm plate were very similar to each other, particularly for 37% and 55% relative densities. In comparison, the pressure-sinkage relationship of the 20.1 cm plate was quite different. In addition to the effect of denser Fillite, it is most likely due to the influence of the pressure bulb effect (Duncan 1998). Any circular plate being pressed into a soil exhibits a "bulb" of pressure with a pressure gradient existing inside the bulb. Per the elasticity solutions provided in Budhu (2007) the increase in vertical stress below the center of uniformly surcharged circular area applied to the top of a soil layer of finite thickness varies from the surcharge pressure at the top to about 6%, 10% and 40% at the bottom of the soil layer (~22.5 cm thick) for the 7.6 cm, 12.6 cm, and 20.1 cm diameter plates, respectively. Therefore, the pressure-sinkage relationship obtained for the 20.1 cm diameter plate was the most and significantly affected by the bottom boundary. Because of this, the test results from the 20.1 cm diameter plate were not used to determine any

model parameters presented later in this paper. For the smaller plate sizes, the thickness of the Fillite specimen was considered to be sufficient.

At the higher densities, particularly for 77.5% relative density, there was a distinct inflection in the pressure-sinkage response immediately following the elastic region of the curve. The 37% relative density tests displayed a smooth upward transition between the elastic and plastic strain regions and 55% relative density test showed inflection, but to a lesser extent in comparison to 77.5% relative density.

The pressure-sinkage results of Fillite were compared to those of other simulants to assess whether Fillite has a greater potential for sinkage in comparison to the other simulants. A significant number of bevameter tests have been conducted on lunar simulant GRC-1 (Oravec 2009) and is a good material to compare to Fillite. Figure 6 compares the range of pressure-sinkage results obtained on GRC-1 by Oravec (2009) for the 12.6 cm plate to that of Fillite, also for the 12.6 cm diameter plate. For the same sinkage displacements, GRC-1 exhibited a much higher resistance. The pressure sinkage data on soils (e.g. ES-3 by Brunskill et al., 2010) showed similar trends. This indicates that Fillite has significantly greater potential for sinkage compared to other terrestrial soil-based simulants.

3.4.2 Parameter Determination and Sinkage Predictions

The pressure-sinkage curves for the 7.6 cm and 12.6 cm diameter plates were used to determine the parameters for Bekker and N2M models described in Sections 1.1 and 1.2, respectively, which are summarized in Table 2. Parameters for the Bekker model were determined using equations 3 - 10 and the parameters for the N2M model were

determined using equations 12 - 14. For the N2M model, a constant value for the sinkage exponent (m) was used because the values only differed slightly between tests. Gotteland and Benoit (2005) conducted extensive tests on a silty sand to determine the sinkage exponent, which was calculated to be 0.8. The average sinkage exponent for Fillite was very close to that at 0.83. Since this conformed well to the already established result for silty sand, this value was used in the prediction model.

The Bekker and N2M prediction models are plotted along with the experimental results in Figure 7. In general, the models matched experimental curves well for both plate sizes and for low to medium densities (37% and 55%). The models are not equipped to capture the inflections and subsequent softening in the pressure-sinkage relationship especially for dense Fillite (77.5% relative density). In general, the N2M model seemed to provide better predictions than the Bekker model. Table 2 also indicates that there is no particular trend in the parameters for the Bekker model, whereas the N2M model parameters generally increase with increasing density, and none of the parameters are negative.

Pressure-sinkage testing has been conducted on several simulants and sands in the past, and model parameters for the Bekker model are available for comparison to Fillite. The Bekker parameters of lunar simulant GRC-1 and Martian soil simulant ES-1 and ES-3 were selected to compare to Fillite as well as parameters for dry sand and sandy. Fillite most closely resembled the Martian simulant ES-1 which was developed by the European Space Agency as a light-weight soil simulant (Brunskill et al., 2010). In general, the exponent *n* for Fillite is less than every other material which demonstrates that the pressure sinkage behavior of Fillite is more non-linear than most of the other materials.

The majority of exponents for each material are close to 1.0, while Fillite stays between roughly 0.3 and 0.7.

Comparisons can be made in a similar fashion for the N2M model as well; however there are no soil simulants that have had N2M parameters determined for them. Gotteland and Benoit (2006) presented values for three different types of soils (frictional soil (F), cohesive soil (C), and frictional-cohesive soil (CF)). In general, the values of the parameters for Fillite were smaller than those of the other soils tested with exception to C_m for sand F and s_m for silt C. The exponential nature of Fillite is similar to that of silty sand CF with an exponent m of 0.83 for Fillite and 0.8 for silty sand.

3.4.3. Application to the Wheels of Spirit Rover

The entrapment of the Spirit rover on Mars (NASA, 2009) is used here as a case study for evaluating the usefulness of Fillite in simulating the high-sinkage scenario experienced by Spirit. Spirit broke through a patch of normal looking soil and four of its six wheels sank in a pocket of Ferric Sulfate, which is thought to have very low cohesion A number of underbelly images of the Spirit rover are also available; they revealed that the four rear wheels were embedded between 50 and 90% of the wheel diameter (NASA, 2009). A 3D simulation of the Spirit rover produced by NASA's Jet Propulsion Laboratory based on numerical prediction results, showed all but the front right wheel (because of the broken actuator) to be embedded to roughly 70% sinkage and greater. The back left wheel was sunk in almost 100% (Trease et al, 2011). Available images of the front two wheels of Spirit rover revealed that the right wheel remained mostly free (the actuator on this wheel was broken) while the left wheel was almost fully embedded in the soil.

The original Bekker model predicts sinkages by approximating the contact area under a wheel as being flat. The Bekker – Wong equation (Wong 2010) is a modification of the original Bekker model that takes into account the wheel geometry. This model uses the same model parameters as the Bekker model, and therefore, it can be used to predict wheel sinkage without the need for a new set of experiments. This mathematical model is written as:

$$\sigma(\theta) = \left(\frac{k_c}{b} + k_\phi\right) r^n (\cos\theta - \cos\theta_1)^n \text{ for } \theta_m \leq \theta \leq \theta_1 \quad (14a)$$

and

$$\sigma(\theta) = \left(\frac{k_c}{b} + k_\phi\right) r^n \left\{\cos\left[\theta_1 - \frac{\theta-\theta_2}{\theta_m-\theta_2}(\theta_1 - \theta_m)\right] - \cos\theta_1)\right\}^n \text{ for } \theta_2 \leq \theta \leq \theta_m \quad (14b)$$

where θ_m denotes the angle to the maximum stress condition, θ_1 is the angle to where the soil first contacts the surface of the wheel at the front of the tire, and θ_2 is the angle to where the soil contacts the wheel at the rear of the tire (Figure 8). All angles are measured from vertical. In this model, *b* is the width of the wheel and *r* is the outer radius of the wheel. All other parameters are taken directly from the Bekker model.

To predict the sinkages of a stationary Spirits wheel, equation 14a was used. For a stationary wheel, θ_1 is symmetric on both sides and is a function of sinkage. By performing a simply geometric conversion, $\cos(\theta_1)$ can be re-written as (r – z)/r. The new simplified model for the sinkage of a stationary wheel becomes:

$$\sigma(\theta) = \left(\frac{k_c}{b} + k_\phi\right) r^n \left(1 - \frac{(r-z)}{r}\right)^n \quad (15)$$

The Bekker parameters used for this model were taken from the normal bevameter tests on Fillite at the lowest relative density (37%). The outer radius (r) and the width (b) of the wheel were taken to be 0.26 m and 0.16 m, corresponding to the wheels

of Spirit rover. The weight was taken as 656.7 N corresponding to the weight of Spirit rover under Mars' gravity. The predicted sinkage was calculated to be 0.221 m in depth, which is roughly 84% sinkage of the wheel diameter. Overall, this predicted sinkage compared well with the actual sinkage experienced by the Spirit rover as seen in Figure 9. A rendering of the Spirit rover's wheel is recreated in Figure 9a with a horizontal plane inserted at 84% of the wheel diameter from the bottom of the wheel. Figure 9b presents an image of the sunken front left wheel of the Spirit rover (NASA, 2009). The two images are very close in appearance, confirming the predicted wheel sinkage based on the parameters derived from Fillite to be quite reasonable.

While the parameters used in this model were selected to predict the maximum sinkage condition, the higher density parameters from the Bekker model can still be used to provide an estimate of the sinkage for various other conditions where the soil is expected to be stronger or denser. While other soil sinkage models exist for vehicle performance prediction, the Bekker - Wong model conclusively demonstrates the high-sinkage/high-slip environment that Fillite can enable. This model also shows that Fillite at its lower densities behaves very similarly to the loose soil that trapped the Spirit rover.

3.5 Shear Bevameter Tests and Results

The normal bevameter test provides insight into the sinkage nature of a granular material by simulating a normal load similar to that of a wheel. A wheel in motion will cause a certain amount of shear deformation within the soil it is operating on as well. The shear bevameter test provides a basis for understanding the interaction between vehicle traction and the granular material in question (Bekker, 1969).

The shear tests conducted on Fillite utilized a shear ring (Figure 10) with an outside diameter of 34 cm and an inside diameter of 27 cm. The ring had grousers spaced every 10 degrees, which extended 15 mm from the bottom surface of the ring. These grousers are used to measure the internal shear strength of the soil by ensuring that the failure plane is beneath the surface of the soil and not between the soil and the ring (Oravec, 2009).

Three separate shear tests were conducted on Fillite using three different normal loads of 100, 200, and 500 N (corresponding to normal stress of 2.98, 5.97, and 14.93 kPa, respectively). This load range was chosen to correspond to the nominal tire loads of the three different rovers sent to Mars (Sojourner, Spirit or Opportunity, and Curiosity) with the weight calculated using Mars' gravity. The normal loads were held constant for each test and the shear ring was rotated at a constant rate of 3 deg/s. All tests were conducted on Fillite with a relative density of roughly 77.5% to assess the shear behavior of Fillite under its near maximum shear strength. Figure 11 shows the results of the shear bevameter tests.

A relationship between the shear stress, τ, and shear displacement, j, was proposed by Janosi and Hanamoto (1961) and is written as:

$$\tau = \tau_{max}\left(1 - e^{-j/K}\right) \tag{16}$$

where τ_{max} is the maximum shear strength of the soil, and K is the shear deformation modulus with units of meters. Because a circular ring was used, the shear deformation was converted to a linear measurement by using the relationship $j=\theta \cdot r$. The average radius between the outer and inner radii of the shear ring was taken as r, and θ was the angle of rotation. K is considered to be a measure of the magnitude of the shear

displacement required to achieve the maximum shear stress of a soil. The maximum shear stress can be computed using equation (Janosi and Hanamoto, 1961):

$$\tau_{max} = c + \sigma_n \tan\phi \tag{17}$$

where c is the cohesion of the soil, σ_n is the normal pressure on the plate, and ϕ is the internal friction angle. The cohesion and friction angle of Fillite were determined in a separate study (Edwards et al, currently under review). In order to determine the value of K, Wong (1980) rearranged equation 16 and used least squares minimization to arrive at a closed form equation:

$$K = \frac{\sum_{i=1}^{n}\left(1-\frac{\tau_i}{\tau_{max}}\right)^2 j_i^2}{\sum_{i=1}^{n}\left(1-\frac{\tau_i}{\tau_{max}}\right)^2 j_i \ln\left(1-\frac{\tau_i}{\tau_{max}}\right)} \tag{18}$$

Calculation of K for each test reveals that the shear deformation modulus decreases with an increase in normal load. The shear deformation modulus for loads of 2.98, 5.97, and 14.93 kPa were calculated to be 0.31, 0.21, and 0.16 m respectively. This makes physical sense as it would be expected that with a larger normal load, less shear deformation would be needed to achieve the maximum shear stress to fail the soil.

It is important to put the magnitude of K for Fillite in order to better understand its shearing behavior, so a comparison was made to the lunar simulant GRC-1. This revealed that the shear deformation modulus K of Fillite is an order of magnitude greater than that of GRC-1, which is a mixture of four sands. Oravec (2009) performed shear bevameter tests on GRC-1 at relative densities ranging between 24 and 56%. Depending on the density, K for GRC-1 ranged from 0.0185 to 0.0255 m for normal loads ranging from 4.80 to 29.01 kPa (Oravec 2009). This suggests that Fillite will deform roughly 10 times as much before reaching its maximum shear strength condition in comparison to GRC-1

or other similar simulant and typical granular soils. Figure 12 presents a comparison between the shear results of Fillite (at about 77.5% relative density) to the shear results of GRC-1 at 55.9% relative density reported by Oravec (2009). Loading the shear ring to 4.99 kPa in GRC-1 produced higher shear stresses than both the 2.98 and 5.98 kPa tests in Fillite. The load of 9.26 kPa in GRC-1 also produced higher shear stresses than a load of 14.91 kPa produced in Fillite.

3.5.1 Comparison of Shear Behavior of Fillite to Spirit Rover Entrapment

A major factor in the Spirit rover being unable to free itself was the high-slip nature of the soil of Mars that entrapped the rover. During attempted evacuation maneuvers, the wheels slipped close to 100% and were unable to gain any traction (NASA 2009). While the exact shear strength parameters of the soil that entrapped the Spirit rover are unknown, it is possible to estimate the values of shear stress and shear deformation caused by the sunken wheels.

Wong and Reece (1967) developed a definition of shear deformation for a wheel in forward rotation as:

$$j_x = r[\theta_1 - \theta - (1 - i)(\sin\theta_1 - \sin\theta)] \quad (19)$$

where j_x is the shear deformation, r is the wheel radius, θ_1 is the soil entry angle (Figure 8), i is the slip coefficient, and θ is a chosen angle between θ_1 and zero. The slip coefficient is a percentage of wheel slip and can be between zero and one. Zero corresponds to zero slip and one corresponds to 100% slip. Similar to the sinkage portion of this study, and angle of zero degrees was chosen in order to investigate the maximum shear stress condition under the wheel as it was stuck. Using the same sinkage

estimations based on the images taken by the Spirit rover (50% – 90% of the wheel diameter), the soil entry angle varies between 1.57 and 2.50 rad. The slip coefficient was taken to be 1.0 as the rover was so deeply embedded and unable to free itself despite numerous attempts. The shear displacements for one of Spirit's wheels embedded between 50% and 90% of its diameter were calculated to be between 0.20 and 0.33 m respectively.

The maximum shear stress of the loose drift soil can next be computed using equation 17. Values of cohesion and internal friction angle of the Martian drift soils have been estimated using visual measurements during both the Pathfinder and Viking missions (Moore et al., 1999; Moore et al., 1982). In order to estimate the strength properties of the soil that entrapped the Spirit rover, the observed soil behavior must be taken into account. The occurrence of a high-sinkage/high-slip situation suggests that the cohesion of the soil was very small. Therefore, the smallest value of cohesion of 0.18 kPa estimated for Martian regolith (Moore et al., 1999) was used in these calculations. It is more difficult to estimate the internal friction angle of the soil, partially because such a wide range of friction angles have been reported from the different missions. Calculations from the Pathfinder lander determined the internal friction angle to range from 15.1˚ to 33.1˚ (Moore et al., 1999). Calculations based on images taken by the Viking landers determined the friction angle of the soil to range from 15.6˚ to 20.4˚ (Moore et al., 1982). It is not necessarily the case that a low cohesive soil will also have a low internal friction angle. For the sake of completeness, the complete range of measured friction angles was used to calculate a range for the maximum shear stress. The last value that needed to be determined is the normal stress on the soil. The normal stress was estimated in the same

way it was estimated for the sinkage prediction, that is by using the known weight of the rover on Mars as well as the geometry of the wheel. The maximum shear stress of the soil directly under a wheel was calculated to range between 1.91 kPa and 4.32 kPa.

Comparing these calculations to the shear measurements of Fillite under a normal load similar to what was applied to the wheels of the Spirit rover reveals that the maximum shear stress of Fillite falls well within the range for Martian soil predicted by equation 17. In order to effectively compare the shear strength of the soft Martian soil to Fillite, equation 16 can be used, but a value for the shear deformation modulus K must be approximated. This parameter is not known for Martian soil so it must be inferred from the estimated behavior of the soil. While the shear deformation modulus is known for simulants such as GRC-1, this study has shown that a much lighter simulant such as Fillite can have a shear deformation modulus roughly an order of magnitude larger. Fillite is currently the only reference material for estimating shear deformation modulus where the weight of the soil is approximately equal to the soil on Mars. Because of this, the K value for Fillite was used for the calculations. This is further justified from the fact that other strength properties of Fillite have been determined to be similar to that of Martian soil, such as cohesion and friction angle (Edwards et al., under review). The shear stresses of Martian soil were calculated using singular values of τ_{max}. Because a range of possible τ_{max} was calculated for Martian soil, a range of shear stresses for the calculated shear deformations is presented in Figure 13.

As expected, a larger τ_{max} corresponds to a larger calculated shear stress in the Martian regolith. The measured shear stress of Fillite at 77.5% relative density falls in the middle of the possible shear stress values estimated to be imparted on the Martian soil by

the Spirit rover's wheels. A relative density of 77.5% was the highest density that was consistently attained for the testing of Fillite, therefore it can be reasonably concluded that the shear stresses for most other Fillite samples will be smaller than what was measured from the shear tests conducted here. This fact can aid the testing of vehicles in large test beds where the density of the Fillite may be unknown.

3.6. Conclusions

This paper presented the results and analysis of normal and shear bevameter tests performed on a simulant called Fillite (grade 500W-LF, off-white in color) made by Tolsa USA, Inc. Fillite is a light, granular material that is also chemically inert and available in large quantities for laboratory studies. Fillite is being used by NASA Glenn Research Center for their test bed in a "sink tank" for rover mobility studies. Suitability of Fillite to simulate high-sinkage, high-slip situation such as the one encountered by the Spirit rover on Mars was examined in this paper.

The results presented here demonstrated that in addition to using a simulant with low strength in physical models, it is also important to match the unit weight of the simulant on Earth to that of Martian (or lunar or other planetary bodies) regolith. Fillite has a specific gravity of 0.67, which is roughly four times smaller than typical granular soils, most Martian and even lunar soil simulants. It also has a bulk unit weight that ranges from 4.07 to 4.67 kN/m^3, which is approximately equal to that of Martial soil. It is slightly larger than the bulk unit weight of lunar soil but is far closer than any other simulant available.

The pressure-sinkage curves of Fillite fell generally below those on other simulants indicating that Fillite has significantly greater potential for sinkage as compared to other terrestrial soil-based simulants. The results of normal bevameter tests were used to determine parameters of the Bekker and N2M models. In general, the N2M model performed better than the Bekker model in predicting the measured pressure-sinkage behavior of Fillite.

A simple estimate of the sinkage of a wheel on the Spirit rover was made using the Bekker parameters of Fillite and the Bekker – Wong model. The predicted sinkage of the Spirit rover wheel in Fillite was 84% of the wheel diameter. This was within the observed sinkage of 50 to 90% of the wheel diameter on Mars.

Fillite demonstrated far lower shearing resistance than GRC-1. This comparison serves as a valuable illustration of the high-slip nature of Fillite.

The results of the shear bevameter tests on Fillite compared well to the estimated shear stresses imparted on the Martian soil by the wheels of the Spirit rover.

Overall, the results presented here showed that Fillite is capable of simulating high-sinkage, high-slip situations for rover studies to be conducted on Earth.

Acknowledgements

This work has been supported by the Vermont Space Grant under NASA Cooperative Agreement #NNX10AK67H. The authors are grateful to Dr. Juan Agui of NASA Glenn Research Center for his advice and general support for the study.

References

Alshibli, K. A., and Aasan, H. "Strength Properties of JSC-1A Lunar Regolith Simulant." *Journal of Geotechnical and Geoenvironmental Engineering;* 2009, 135.5: 673.

Bekker, M. G. *Introduction to Terrain-vehicle Systems*. Ann Arbor: U of Michigan, 1969.

Bekker, M. G. *Theory of Land Locomotion; the Mechanics of Vehicle Mobility*. Ann Arbor: U of Michigan, 1956.

Bin, C., Jianqio, L., Yinwu, L., "Pressure-sinkage Model and Experimental Research of Interaction Between Rigid-wheel and Simulant Lunar Soil". *Intelligent Vehicles Symposium*, 2009.

Brunskill, C., Patel, N, Gouache, T. P., Scott, G. P., Saaj, C. M., Matthews, M., and Cui, L. "Characterisation of Martian Soil Simulants for the ExoMars Rover Testbed." *Journal of Terramechanics*; 2011, 48.6: 419-38

Budhu, M. Soil Mechanics and Foundations, John Wiley & Sons, Inc., 2nd edition; 2007.

Duncan, C. I. *Soils and Foundations for Architects and Engineers*. 2nd ed. New York: Van Nostrand Reinhold; 1998.

Edwards, M., Dewoolkar, M., Huston, D. "Geotechnical Propertied of Fillite – a Simulant for High-Slip/High Sinkage Rover Mobility Studies." *Journal of Aerospace Engineering.* Currently under review; 2014.

Goriatchkin, B. "Teoria I Proisvodstvo Sielskohoziaynih Mashin." *Collective Work*; 1937.

Gotteland, P., and Benoit, O. "Sinkage Tests for Mobility Study, Modelling and Experimental Validation." *Journal of Terramechanics*; 2006, 43.4: 451-67.

Heiken, G., Vaniman, D., and French, B. M.. *Lunar Sourcebook: A User's Guide to the Moon*. Cambridge: Cambridge UP; 1991.

Janosi, Z., Hanamoto, B., "*The Analytical Determination of Drawbar Pull as a Function of Slip for Tracked Vehicles in Deformable Soils*", Proceedings of the 1st International Conference on the Mechanics of Soil-Vehicle Systems, Edizioni Minerva Tecnica, Torino, Italy; 1961.

Kulhawy, F. H., and Mayne, P. W. "Manual on Estimating Soil Properties for Foundation Design, Report EPRI EL-6800", prepared for Electric Power Research Institute; 1990.

Lindemanne, R., "*Broader Interests and Applications: The view of a JPL Hardware Engineer",* XTerramechanics: Integrated Simulation of Planetary Surface Missions, CalTech; 2011

McKee, Maggie. "Mars Rover May Not Escape Sand Trap for Weeks." *New Scientist*. 12 May; 2009.

Meirion-Griffith, G., and Spenko, M. "A Modified Pressure–sinkage Model for Small, Rigid Wheels on Deformable Terrains." *Journal of Terramechanics*; 2011 48.2:149-55.

Moore, H. J., Clow, G. D., and Hutton, R. E. "A Summary of Viking Sample-Trench Analyses for Angles of Internal Friction and Cohesions." *Journal of Geophysical Research*; 1982, 87.B12: 10043-0050.

Moore, H. J., Bickler, D. B., Crisp, J. A., Eisen, H. J., Gensler, J. A., Haldemann, A., Matijevic, J. R., Reid, L. K., and Pavlics, F. "Soil-like Deposits Observed by

Sojourner, the Pathfinder Rover." *Journal of Geophysical Research*; 1999, 104.E4: 8729-746.

NASA, "*Spirit and Opportunity Mission News"*, http://www.nasa.gov/mission_pages/mer/freespirit.html, 2009. Last accessed August 6, 2014.

Oravec, Heather Ann. *Understanding Mechanical Behavior of Lunar Soils for the Study of Vehicle Mobility*. Thesis. Case Western Reserve University, 2009.

Peters, G. H., Gregory, W. A., Bearman, H., Mungas, G.S., Smith, J., Anderson, R. C., Douglas, S., and Beegle, L. W. "Mojave Mars Simulant—Characterization of a New Geologic Mars Analog." *Icarus,*; 2008, 197.2 : 470-79.

Trease, B., Arvidson, R., Lindemann, R., Bennett, K., Zhou, F., Iagnemma, K., Senatore, C., Van Dyke, L. "Dynamic modeling and soil mechanics for path planning of Mars Exploration Rovers." Paper presented at the *ASME Design Engineering Technical Conference*, Washington, DC; 2011.

Wong, J. Y., and Reece, A. *"Prediction of Rigid Wheel Performance Based on the Analysis of Soil-wheel Stresses. Part I. Performance of Driven Rigid Wheels*". Journal of Terramechanics; 1967, 4(1), 81–98

Wong, J. Y. "Data Processing Methodology in the Characterization of the Mechanical Properties of Terrain." *Journal of Terramechanics*; 1980, 17.1 : 13-41.

Wong, J. Y. "Terramechanics and Off-road Vehicle Engineering: Terrain Behaviour, Off-road Vehicle Performance and Design". *Amsterdam: Butterworth-Heinemann*; 2010.

Table 3.1. Index and Strength Property comparison of Fillite to Martian and Lunar soils and simulants ([1]Moore 1999; [2]Moore and Clow 1982; [3]Heiken et al.,1991).

Soil Properties	Fillite	Martian Soil		Lunar Soil[3]
		Pathfinder[1]	Viking 1 & 2[2]	
Median Particle Size, D_{50} (mm)	0.18	-	-	0.04-.13
D_{10} (mm)	0.13	-	-	0.013
D_{30} (mm)	0.2	-	-	0.034
D_{60} (mm)	0.21	-	-	0.14
Coefficient of Uniformity, C_u	1.62	-	-	10.769
Coefficient of Curvature, C_c	1.47	-	-	0.635
Maximum Bulk Density, ρ_{max} (kg/m^3)	476.1	1518	1300	1810
Minimum Bulk Density, ρ_{min} (kg/m^3)	415.4	1285	1000	920
Specific Gravity, G_s	0.669	-	-	2.3-3.2
Bulk Unit Weight (kN/m^3), γ	4.07-4.67	4.77-5.63	3.71-4.82	1.49-2.94
Maximum Void Ratio, e_{max}	0.61	-	-	1.8
Minimum Void Ratio, e_{min}	0.405	-	-	0.712
Maximum Porosity, n_{max}	0.379	-	-	0.97
Minimum Porosity, n_{min}	0.288	-	-	0.416
Compression Index, c_c	0.041	-	-	0.012-0.108
Recompression index, c_r	0.014	-	-	0-0.013
Peak Friction Angle, ϕ_p (deg)	33.0-37.3	15.1-33.1	15.6-20.4	30-50
Peak Cohesion, c_p (kPa)	1.2-4.6	0.21	0.4-2.8	0.4
Critical Friction Angle, ϕ_{cs} (deg)	32.9-36.4	-	-	-
Critical Cohesion, c_{cs} (kPa)	0-2.4	-	-	-
Dilatancy Angle, ψ (deg)	7.1-24.5	-	-	-
Young's Modulus, E_{ur} (MPa)	19.6-73.2	-	-	-
Poisson's Ratio, υ	0.3-0.41	-	-	-
Small-strain Shear Wave Velocity, v_s (m/s)	126.6-277.8	-	-	40-400
Small-strain Shear Modulus, G_{max} (MPa)	6.9-35.5	-	-	1.47-289.6

Table 3.2. Model parameters for the Bekker and N2M models.

Relative Density (%)	Bekker Parameters			N2M Parameters			
	n	k_c (p/L^{n-1})	k_ϕ (p/L^n)	C_m (pL^m)	s_m (pL^{-m})	s_0 (p)	**m**
37	0.71	-9.26	216.2	0.32	126.1	68.75	0.83
55	0.58	2.11	84.0	0.89	152.69	179.5	0.83
77.5	0.33	-4.61	116.1	0.58	274.4	269.65	0.83

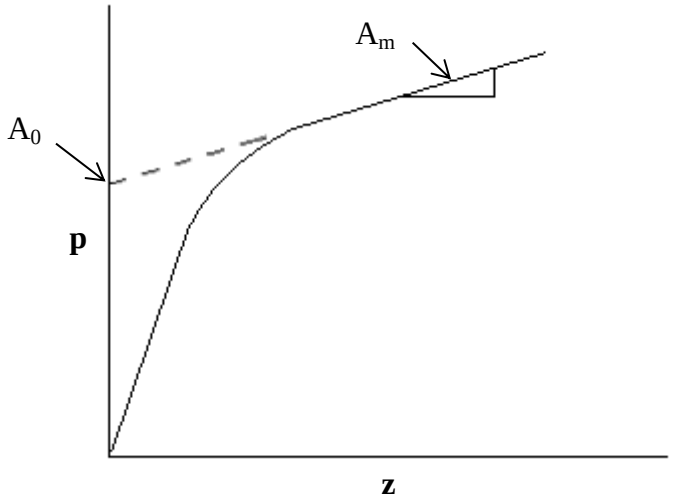

a)

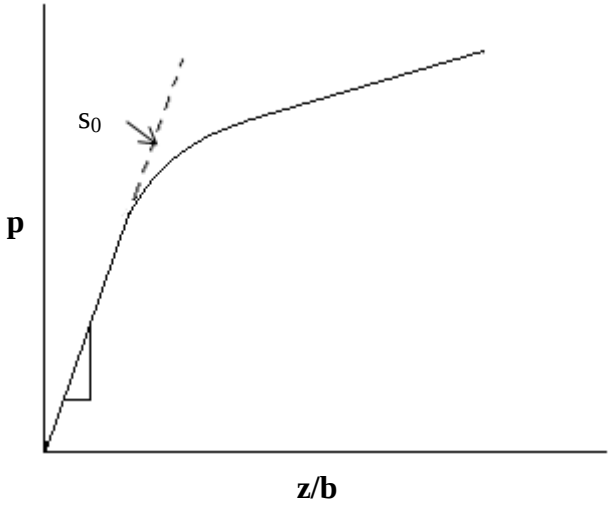

b)

Figure 3.1. a) Parameter determination of A_0 and A_m in the N2M model. b) Determination of s_0 in the N2M model with pressure, p, displacement, z, and normalized displacement, z/b.

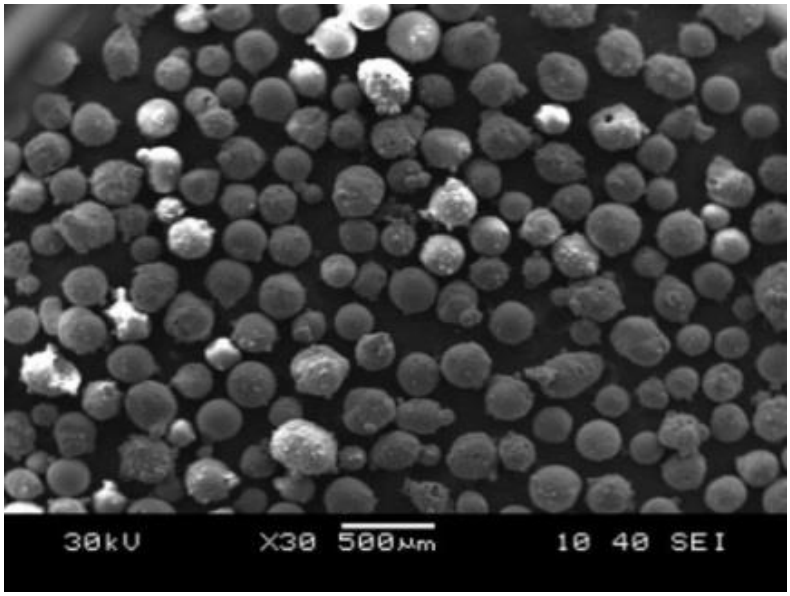

Figure 3.2. SEM image of Fillite at 30x magnification.

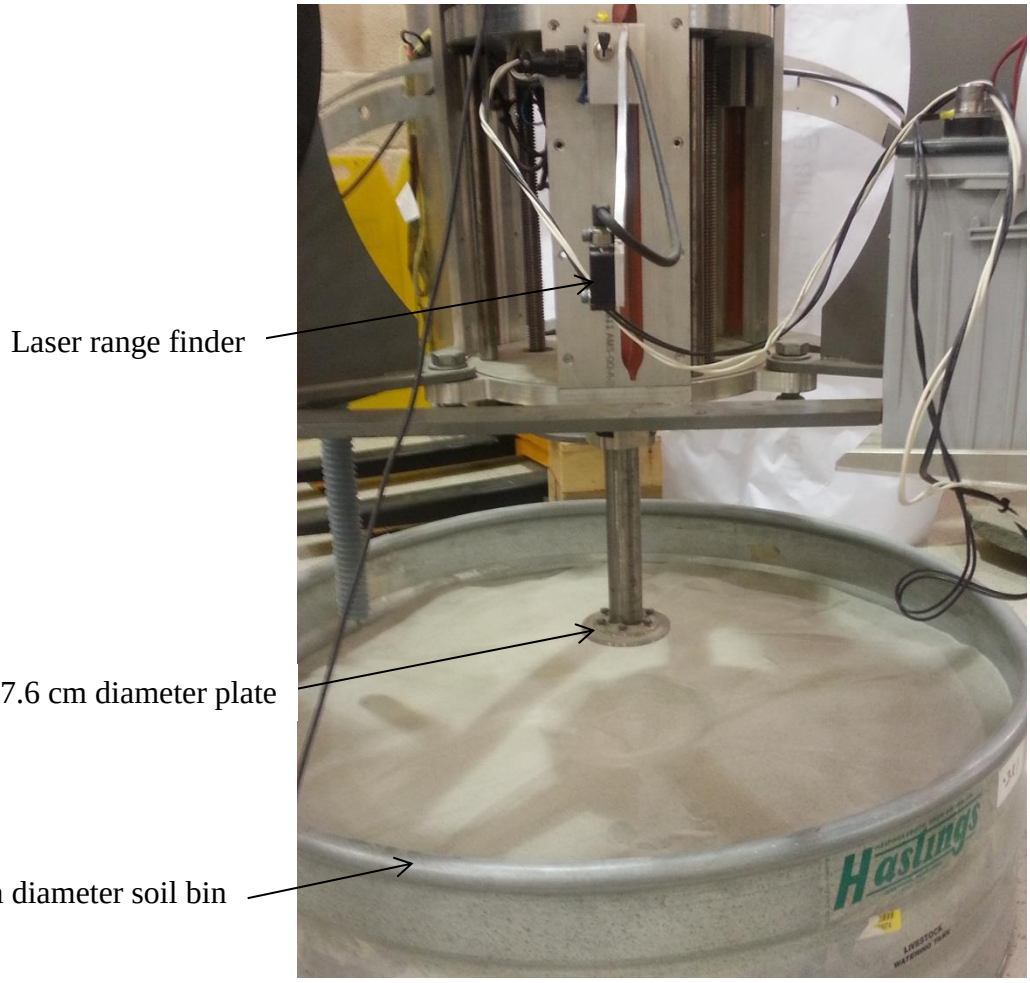

Figure 3.3. Bevameter test setup.

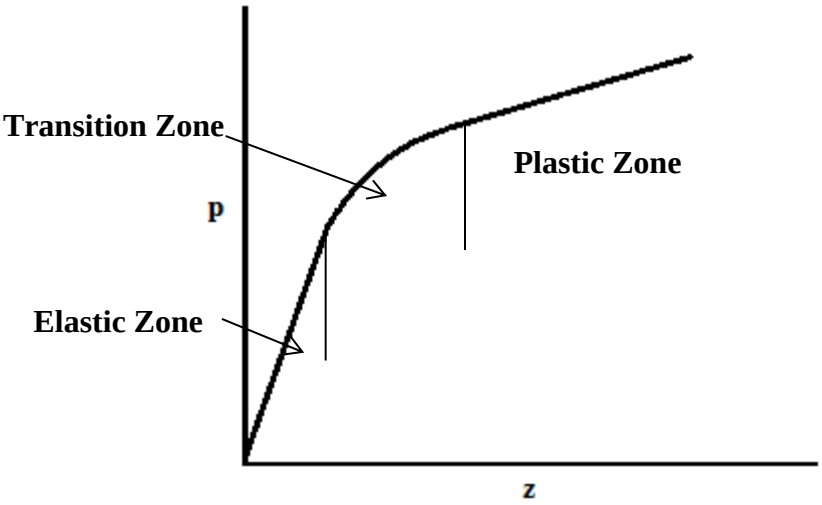

Figure 3.4. Typical pressure-sinkage curve as suggested by Gotteland and Benoit (2006).

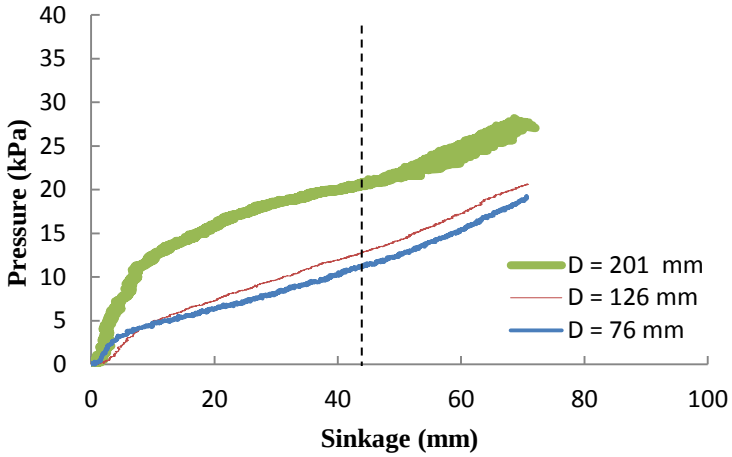

a) D_r = 37%

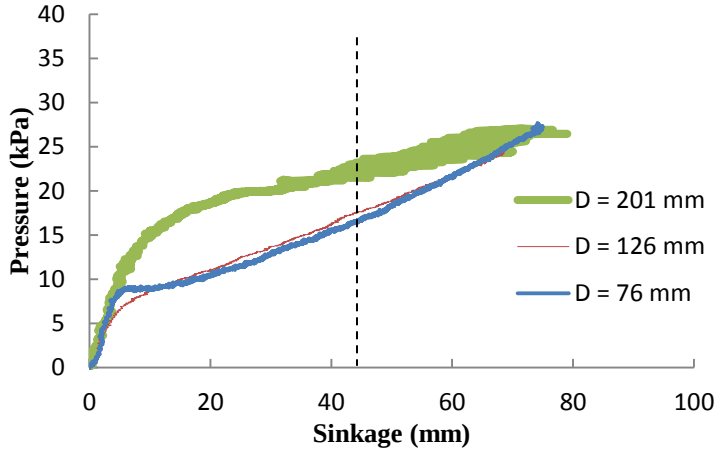

b) D_r = 55%

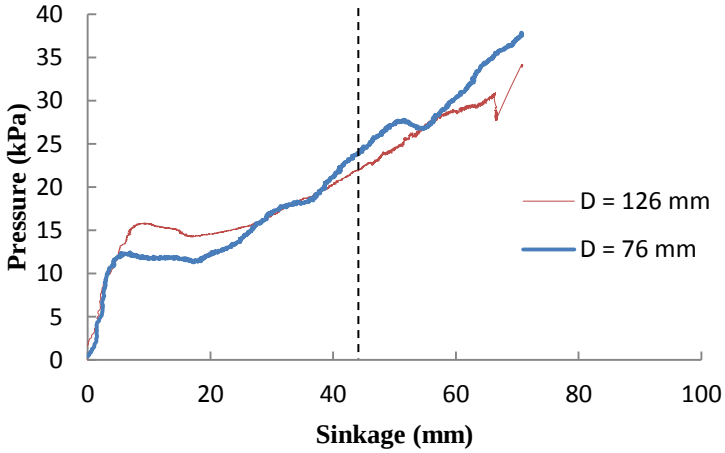

c) D_r = 77.5%

Figure 3.5. Pressure-sinkage curves of Fillite for three relative densities (D_r) and three plate diameters (D). The vertical line indicates the "rule of five" depth.

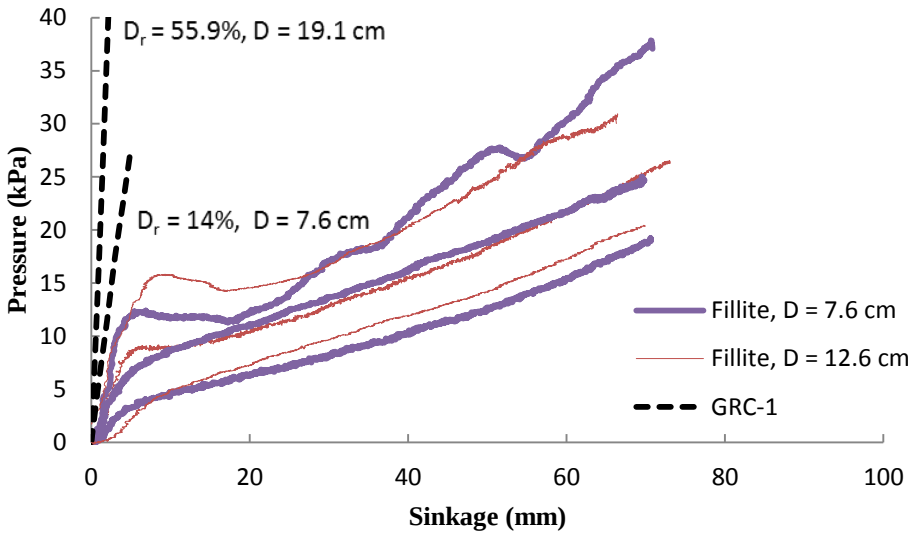

Figure 3.6. Comparison of the pressure-sinkage curves of Fillite to that of GRC-1. The dotted black lines trace the upper and lower bounds for GRC-1 (Oravec, 2009).

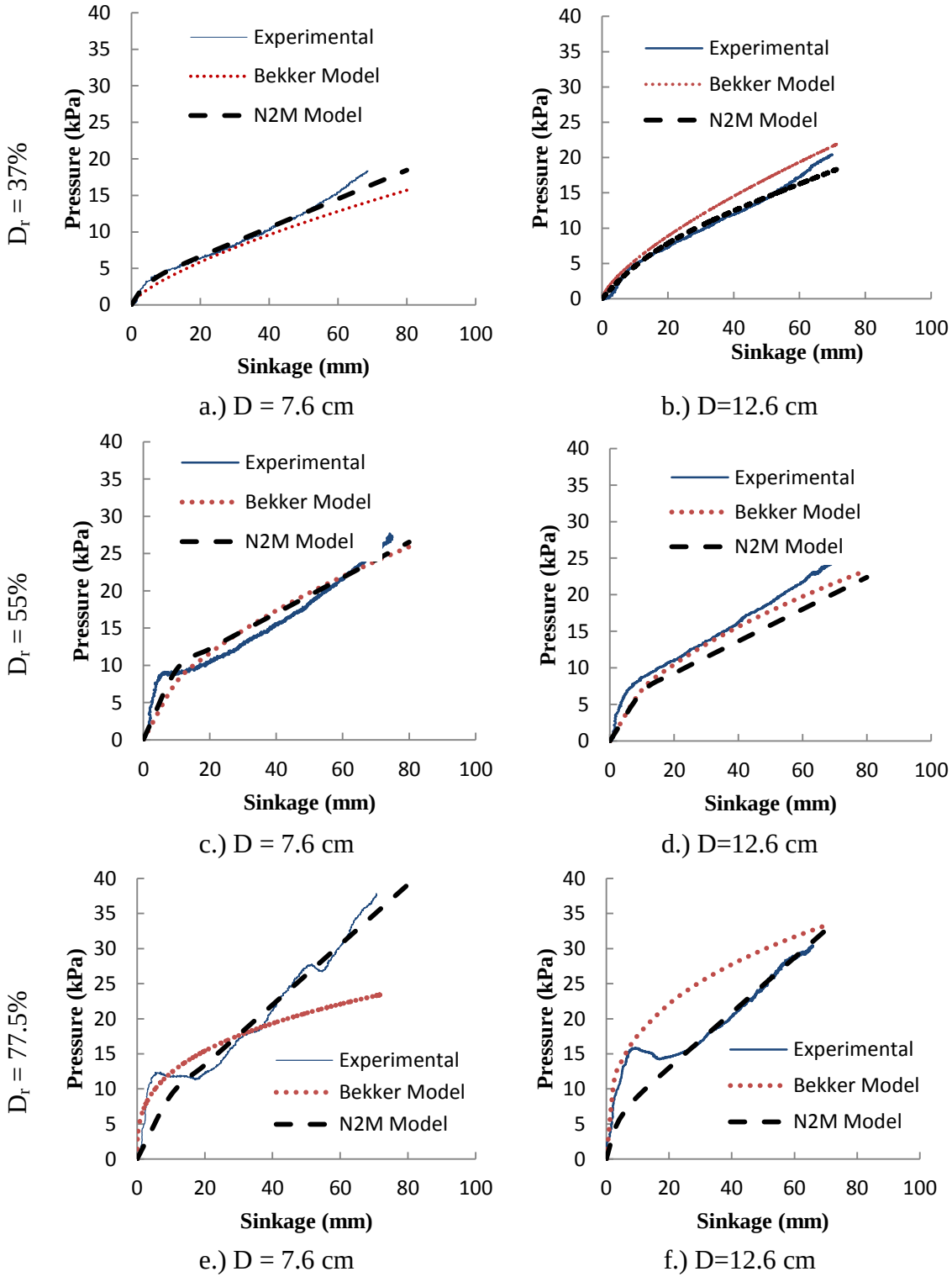

Figure 3.7. Prediction models for Fillite

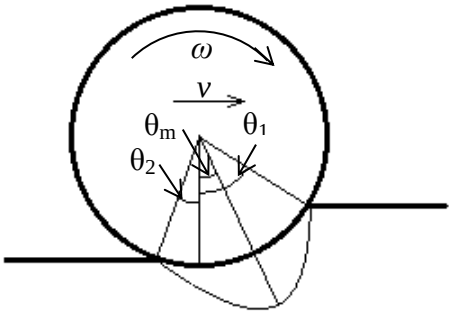

Figure 3.8. Diagram of a rolling wheel in soil.

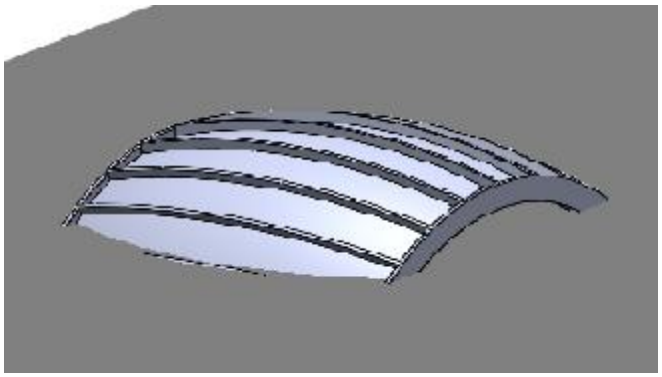

a)

b)

Figure 3.9. Visual comparison between a.) the predicted sinkage depth covering 84% of the wheel, and b.) the embedded front left wheel of the Spirit rover as seen inside the oval (NASA, 2009).

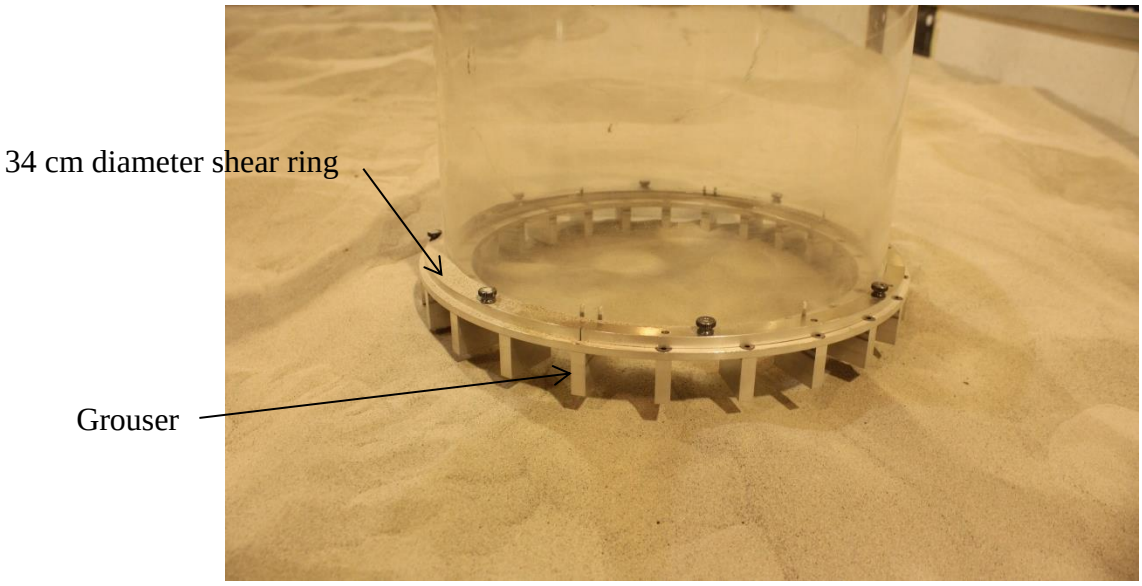

Figure 3.10. The shear ring being inserted into Fillite.

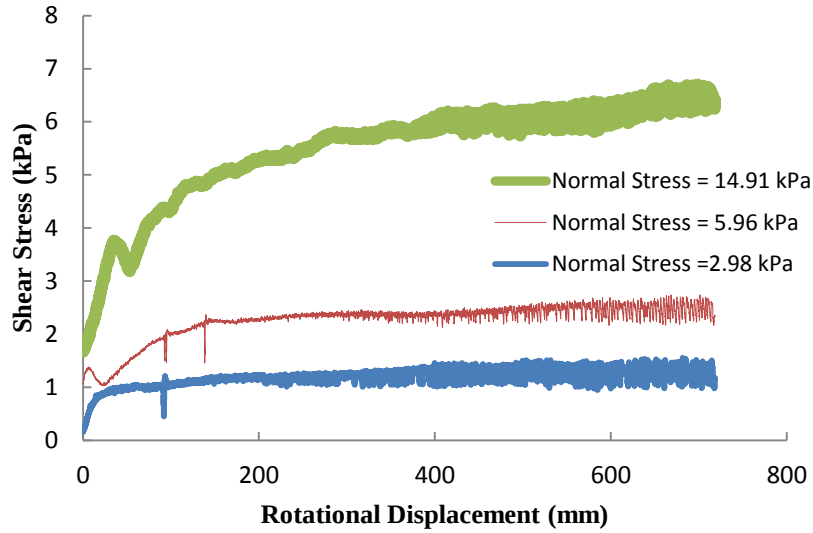

a.)

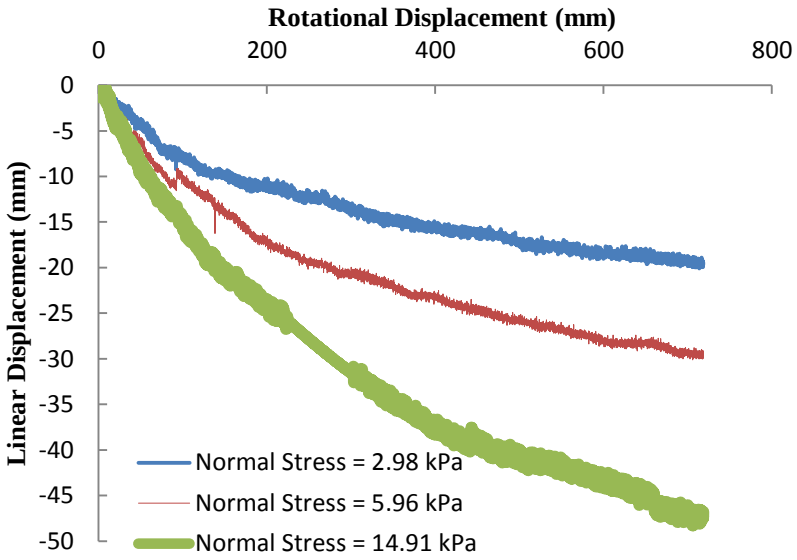

b.)

Figure 3.11. Shear bevameter results for Fillite

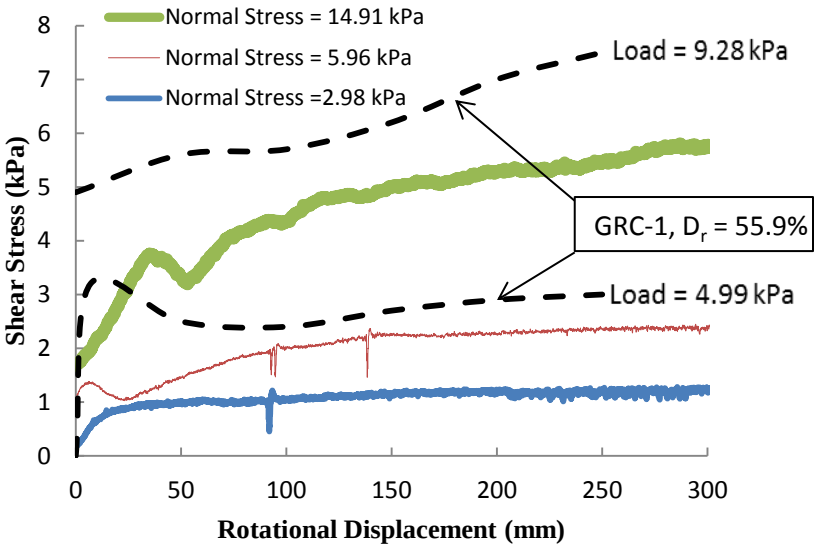

Figure 3.12. Comparison between the shear stresses measured in Fillite and GRC-1 from the shear bevameter test.

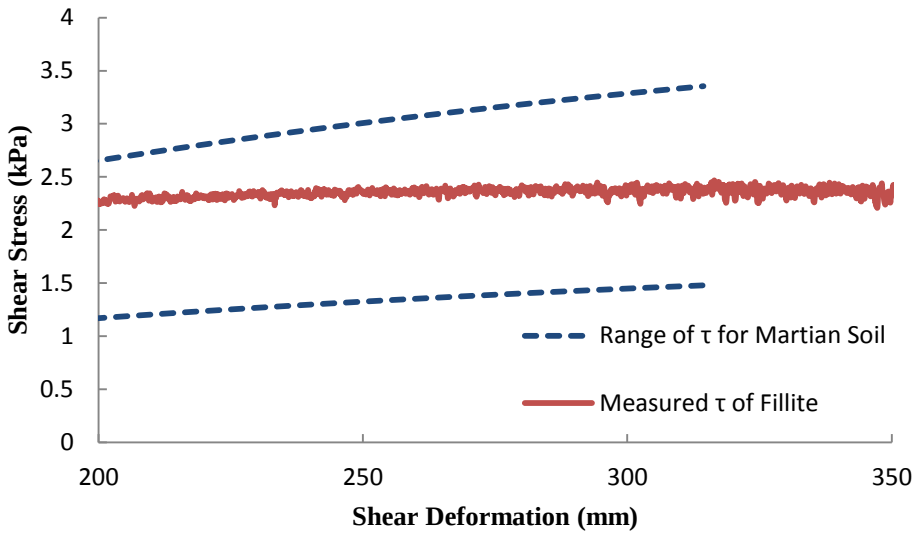

Figure 3.13. Comparison of possible shear stresses of Martian soil to the shear stress of Fillite.

CHAPTER 4: CONCLUSION AND FUTURE WORK

4.1 Conclusions

This thesis presented the results of a research program evaluating suitability of a simulant called Fillite for simulating high-sinkage/high-slip rover mobility conditions on Mars and the Moon. Standard geotechnical material properties such as bulk density, specific gravity, compression index, Young's modulus, and Poisson's ratio were determined from a series of laboratory tests which were performed in general accordance to ASTM standards when available. Tests were also performed to determine some less standard material properties such as the small-strain shear wave velocity and maximum shear modulus. Bevameter testing was also performed to determine model parameters of select pressure-sinkage models. The results of bevameter testing were extended to model the situation that entrapped the Spirit rover on Mars.

The results of this experimental investigation support the conclusion that Fillite is a suitable material for simulating the high-sinkage and high-slip environments that could be experienced on the surface of Mars and potentially on the Moon. In addition, the following specific conclusions are drawn from this study:

1. The particle size distribution of Fillite falls outside the range of the loose drift material on Mars that was determined by Viking 1 but is within the range of the blocky surface material. The drift material particle size ranged from 0.0001 to 0.01 mm while the blocky material ranged from 0.0001 to 1.5 mm.
2. Although the specific gravity is not known for Martian regolith for comparison purposes, the unit weight of Fillite falls well within the range

of unit weight of Martian regolith estimated by Viking and just outside the range based on Pathfinder. Using a Martian soil simulant that weighs the same in Earth's gravity as Martian soil weighs in Mars' gravity could allow researchers and engineers to develop vehicles and structures that are much better prepared to perform as intended on the surface of Mars. Fillite may also have its benefits for lunar regolith simulation as well since many of its properties are similar to lunar regolith and its unit weight is much closer to lunar regolith than most lunar simulants currently in use.

3. The internal friction angle of Fillite compared well with that estimated by Pathfinder, but was considerably higher than what was calculated using the data from the Viking landers. Conversely, the cohesion of Fillite was found to be much closer to what was inferred by the Viking landers but was much higher than what was estimated with Pathfinder data. The discrepancies between Pathfinder and the Viking landers are most likely due to the fact that neither had the ability to directly measure these properties, but rather had to infer them from various images and other tests. Nonetheless, the strength properties of Fillite correspond to values estimated by at least one of the explorations of the lander.
4. The compression index of Fillite is lower than other lunar simulants but still falls within the range of lunar soil. The recompression index is larger than other simulants but is approximately equal to the largest value that was measured on lunar soil. No compression data is currently available on

Martian soil, but it can be concluded that Fillite behaves similarly to lunar soil under one dimensional compression conditions.

5. The shear wave velocity of Fillite ranged from 126.6 m/s at the lowest density (~20%) and confining pressure (12.5 kPa) to 277.8 m/s at the highest density (~75%) and confining pressure (150 kPa). The maximum shear modulus ranged from 6.9 to 39.5 MPa.
6. The pressure-sinkage curves determined for Fillite through normal bevameter testing fell generally below those on other simulants indicating that Fillite has significantly greater potential for sinkage as compared to other terrestrial soil-based simulants. The results of normal bevameter tests were used to determine parameters of the Bekker and N2M models. In general, the N2M model performed better than the Bekker model in predicting the measured pressure-sinkage behavior of Fillite.
7. A simple estimate of the sinkage of the Spirit rover's wheel was made using the Bekker parameters of Fillite and the Bekker – Wong model. The predicted sinkage of the Spirit rover wheel in Fillite was 84% of the wheel diameter. This was within the observed sinkage of 50 to 90% of the wheel diameter on Mars.
8. Fillite demonstrated far lower shearing resistance than GRC-1. This comparison serves as a valuable illustration of the high-slip nature of Fillite.

9. The results of the shear bevameter tests on Fillite compared well to the estimated shear stresses imparted on the Martian soil by the wheels of the Spirit rover.

In summary, Fillite has many physical and mechanical properties that are similar to what is known about Martian regolith. Comparing properties of Fillite to lunar regolith when properties of Martian regolith are not well known still yields comparable results. Also, because Fillite is light-weight, readily available, chemically inert, and can be reused after anticipated applications related to rover mobility studies, it is a suitable simulant for rover mobility studies applicable to Mars and the Moon. Fillite is quite dilatant; its peak and critical angles of internal friction are smaller than those of most other simulants. Smaller shear strength, coupled with much smaller bulk unit weight as compared to other simulants, results in smaller bearing and shearing resistances allowing for better simulation of the intended high-sinkage, high-slip situations for rover mobility studies to be performed on Earth. This was confirmed through normal and shear bevameter testing and analysis of their results.

Whenever possible, simple empirical correlations relating mechanical properties (elastic modulus, dilatancy angle, secant peak friction angle, small-strain shear wave velocity, and maximum shear modulus) of Fillite as a function of the state (relative density or void ratio) and confining pressure were provided so these properties can be readily estimated to support further analytical studies.

4.2 Suggestions for Future Work

Recommendations for future work on Fillite may include but are not limited to:

- Conducting sinkage tests using wheels of various sizes and geometries would be beneficial. While the prediction model presented in this study demonstrated the high sinkage nature of Fillite, a more comprehensive approach can be used for observing wheel sinkages on actual wheels. Different wheel geometries and different loading conditions could be used to better predict sinkages of future rovers.
- Developing a method of controlling the density of Fillite in large test beds would be beneficial. This will also be useful for conventional pressure sinkage tests as well. Using a larger test bed is the best way to eliminate any boundary effects that may be present, but these test beds would have to be homogeneous.
- Sophisticated numerical models have been developed to simulate rover mobility on Mars, but many of the Martian soil properties are still unknown. The properties of Fillite could be incorporated into these models to further validate the sinkage behavior of Fillite and its use as a Martian soil simulant.
- Determination of the static charging properties of Fillite would help to better understand strength properties such as cohesion and grain to grain interactions. Because the particles of Fillite are so light, any static charge on a particles surface can cause numerous grains to stick together.
- Identification of ways to modify the mechanical properties of Fillite for other testing regimes, while maintaining the desirable low specific weight of unmodified Fillite.

APPENDIX A: CONE PENETRATION TEST RESULTS

The cone penetration test (CPT) is a popular in situ test for subsurface investigations. The test is performed by pushing a penetrometer rod with a conical tip (60^o apex angle, 35.7 mm diameter with 1000 mm^2 cross-sectional area, 133.7 mm long cylindrical sleeve with 15,000 mm^2 surface area) into the ground at a standard rate of 20 mm/s. The measured point or tip resistance is designated as q_c and the measured side or sleeve resistance is designated as f_s. A load cell is located just above the cone tip to measure the tip resistance of the cone as it penetrates the soil. Another loadcell is used to infer the sleeve resistance.

A limited number of cone penetration tests were conducted on Fillite to gain insight into its penetration resistance. In this investigation, a miniature cone penetrometer was used. This penetrometer was a piezocone, which provides the ability to measure pore pressure; but since Fillite was tested in dry condition, pore pressure measurement is irrelevant. The miniature laboratory cone penetrometer (type CONE, A01F0.5CKEW2, 50 bar) was 11.3 mm in diameter (10 mm^2 cone cross-sectional area), with a 43.5 mm long sleeve (1,500 mm^2 surface area) made by Fugro Engineers B.V. The cone penetrometer is 747 mm long.

A driving mechanism and associated software was designed and built in-house at the University of Vermont. The driving mechanism allows the cone penetrometer to be pushed in a soil sample at variable rates. In this work, a rate of penetration of 20 mm/s was used. The cone was pushed in a triaxial specimen of 152.4 mm (6") diameter and about 320 mm (12.6") high triaxial specimens of Fillite. Photographs of the cone penetrometer, driving mechanism and the setup including the triaxial cell are included in Figure A.1.

A total 7 cone penetration tests on Fillite were completed at relative densities of 28%, 58% and 72.3%. A set of cone penetration tests was completed for a relative density of 72.3% with three confining pressures of 50, 100, and 150 kPa. Two tests were completed for 58% relative density with confining pressures of 50 and 100 kPa, and one test at 28% relative density was conducted at 100 kPa. The test results for all of the completed tests are presented in Figure A.2. The sleeve friction results are only plotted after 100mm due to the fact that the sleeve is 100 mm long. This ensures that the data is only shown when the sleeve was completely submerged.

Several cone penetration tests were conducted on Ottawa sand in order to get a baseline comparison between a regular fine sand and Fillite. Although the relative densities of these tests were not known, they were prepared to achieve the highest density possible. These tests saw tip pressures of roughly twice as high as Fillite for the same confining pressures.

It is recognized that the cone penetration measurements made here were done on a significantly smaller miniature piezocone and the specimen size was comparatively small as compared to the recommended specimen diameter to cone diameter ratio. For example, Bolton, et al. (1999) and Katagiri and Okamura (2000) recommended the specimen diameter to cone diameter ratio of 40, and in the testing presented here this ratio was 13.5. Also, some of the CPT literature is based on rigid wall calibration chamber tests where the soil specimens were under anisotropic stress conditions. The tests presented here were done under flexible wall, triaxial specimens under isotropic confining conditions. Nonetheless, the results obtained on Fillite are compared to the results available in the literature.

Mayne et al (2001) presented a relationship between relative density (D_r) and the normalized tip stress of the cone (q_{T1}). The normalized tip stress can be calculated using the following equation:

$$q_{T1} = q_c/(\sigma_{vo}')^{0.5} \quad (1)$$

where q_c is the tip stress in atm and σ_{vo}' is the confining stress in atm. The mathematical relationship is written as (Mayne et al, 2001):

$$D_r = \sqrt{\frac{q_{T1}}{300 \cdot OCR^{0.2}}} \quad (2)$$

where *OCR* is the over consolidation ratio. This relationship was developed for clean quartz sand so it was expected that Fillite will have a lower measured normalized tip stress than what would be predicted by equation 1. This is confirmed in Figure A.3 where tip stresses for Fillite fall well outside the predicted curve developed for Quartz sand.

An empirical relation was also developed by Robertson and Campanella (1983) for predicting the effective friction angle of the soil using only the normalized tip stress. For this equation, the normalized tip stress is defined as q_t/σ_{vo}'. The equation is written as (Robertson and Campanella, 1983):

$$\phi' = \tan^{-1}[0.1 + 0.38\log(q_t/\sigma_{vo}')] \quad (3)$$

This equation was developed using cone penetration data from five separate types of sands (Robertson and Campanella, 1983). In order to compare the accuracy of this predictive equation to Fillite, the peak friction angle values of Fillite were calculated using equation 13a in chapter 2. This is an empirical equation based on the peak friction angle calculations from the triaxial test results. This equation is dependent on the critical friction angle as well. Since these values are unknown for the specific relative densities used for the cone tests, interpolation was used to estimate the critical state friction angles.

Figure A.4 presents a comparison between the Robertson and Campanella equation for peak friction angle and the values calculated for Fillite using equation 13a in chapter 2. The internal friction angles calculated for Fillite were fairly close to the Robertson and Campanella prediction, but remained slightly higher for each tip stress. This indicates that Fillite has friction angles smaller than, but fairly similar, to those of traditional sands.

References

Bolton, M. D., Gui, M. W., Garnier, J., Corte, J. F., Bagge, G., Laue, J., and Renzi, R. "Centrifuge cone penetration tests in sand", *Geotechnique*; 1999, 49(4), 543-552.

Katagiri, M., and Okamura, M. "Manual of basic centrifuge tests, 4. Cone penetration test, Proc. International Conference *Centrifuge 9;* 2000, Vol. 2, 1059-1066.

Mayne, P. W., Christopher, B. R., DeJong, J., "Subsurface Investigations – Geotechnical site Characterization". *National Highway Institute*; 2002, pg 9-12 to 9-15. Publication No. FHWA NHI-01-31

Robertson, P.K. and Campanella R. G. "Interpretation of cone penetration tests: PartI – sands; part II – clays". *Canadian Geotechnical Journal*; 1983, Vol. 20 (4), 719-745.

(a) Cone penetrometer

(b) Driving mechanism

(c) Test set-up

Figure A.1. Cone penetration test set-up

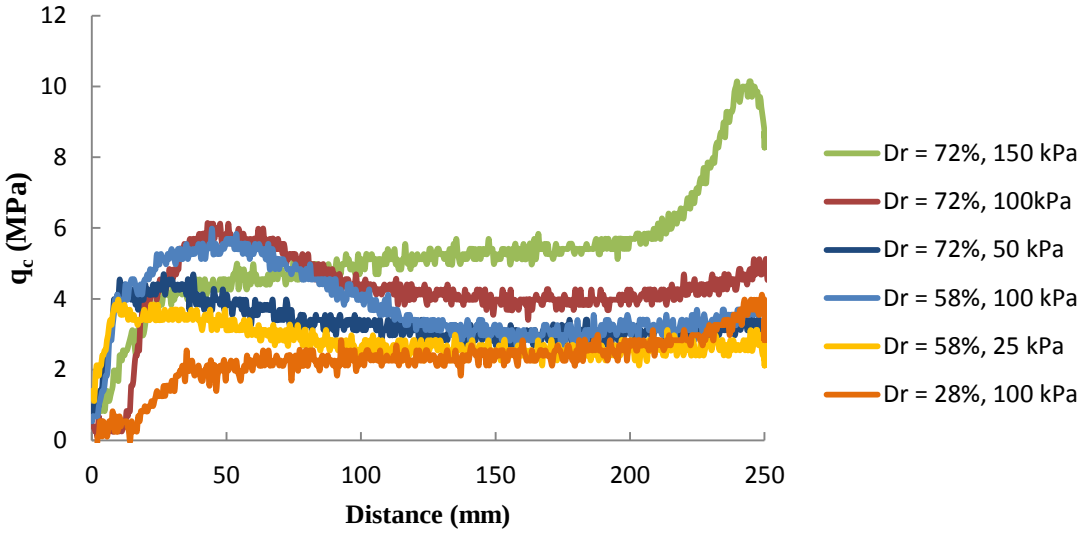

(a) Normal tip stress.

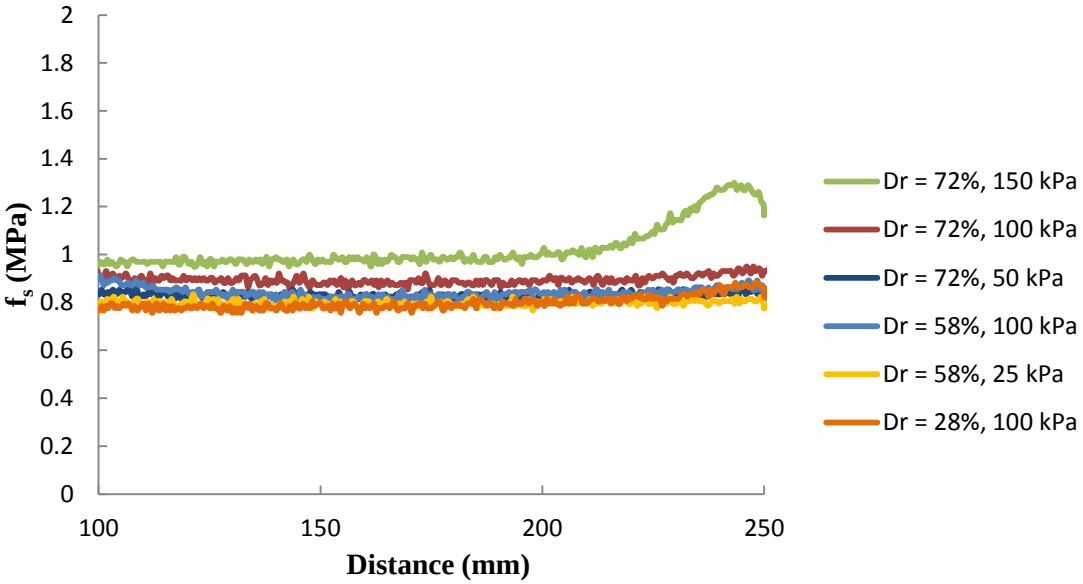

(b) Sleeve friction.

Figure A.2. Cone test results for Fillite

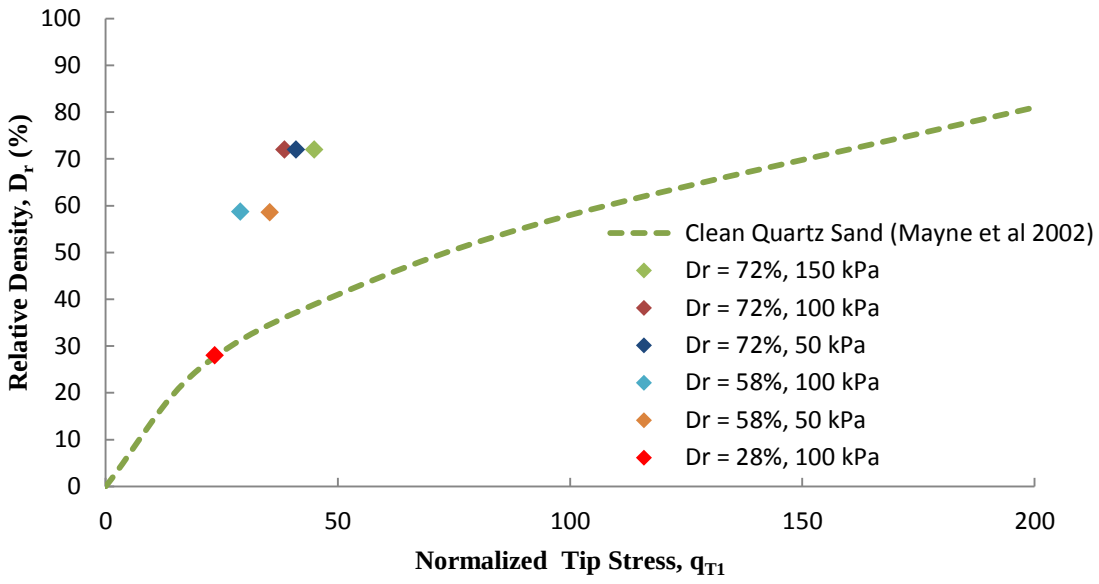

Figure A.3. Measured nominal tip stresses of the cone in Fillite compared to the c curve of clean quartz sand.

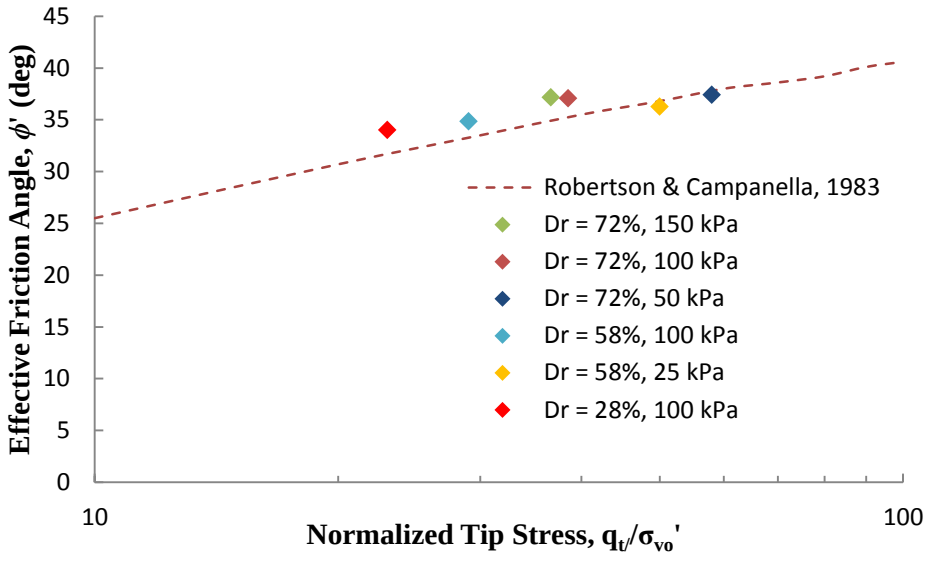

Figure A.4. Effective friction angle of Fillite estimated by equation 3.

APPENDIX B: TRIAXIAL TEST SETUP

B.1 Equipment

- Membrane

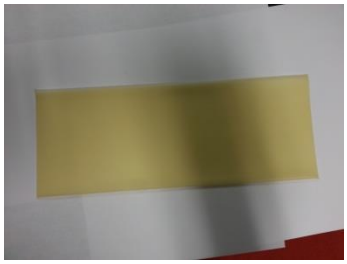

- O-rings x 6

- Porous stone x 2

- Filter paper x 2

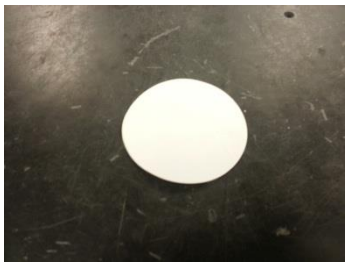

- Base

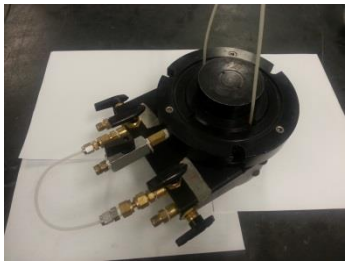

- Top cap

- Mold

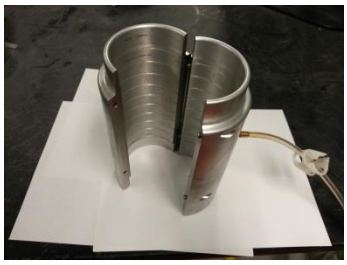

- Mold clamp

- Collection Pan

- Pressure chamber

- Piston

- Support rod x 3

- De-aerator

B.2 Instructions For Setting Up Triaxial Test On Dry, Granular Specimen

1. Turn on the vacuum pump and fill up the water deaerator until the water is between the marks on the glass.

2. Shut off the intake valve and plug in the deaerator so the disk at the bottom begins to spin. Leave the vacuum pump on.

3. Leave the on deaerator for now.

4. Apply vacuum grease around the groove on the top cap, the groove on the

base and six o-rings.

5. Put the membrane on the base such that the bottom of the membrane is flush with the lower surface of the base.
6. Apply three of the o-rings to secure the membrane to the base. One o-ring should be in the groove with 2 below it.
7. Wipe down the inside of the mold halves.
8. Apply grease down the contact surfaces of both mold halves.
9. Place the mold around the membrane. Make sure that the membrane is not pinched by the mold.
10. Place the mold clamp around the mold and tighten the nut down.
11. Fold the membrane over the mold.
12. Place a porous stone in the membrane such that it is flush with the bottom.
13. Put filter paper on top of the stone.
14. Weigh the current setup with all of the parts (top cap, rest of the o-rings with grease, porous stone, and filter paper).
15. Remove from scale and put on the collection pan.
16. Apply vacuum to the mold. Use up to 20 kPa.
17. Place on respirator.
18. Weigh out each soil layer and pour into membrane. Tap down soil layers if necessary.

19. When all soil is in membrane, remove the collection pan.

20. Place filter paper on top of soil.

21. Place porous stone on top of filter paper.

22. Place top cap on top of the stone.

23. Fold up the membrane.

24. Place the remaining o-rings around the top cap.

25. Clean the base of the mold thoroughly.

26. Attach tubes to the top cap.

27. Seal off the vacuum and remove the vacuum tube.

28. Weigh the final setup.

29. Hook up vacuum to the left most valve on the base. Make sure the middle two valves are open and the right most valve is closed. Vacuum should be under 20 kPa.

30. Remove the mold.

31. Measure the diameter of the sample in four places.

32. Measure the height of the sample in four places.

33. Apply grease to the top and bottom of the pressure chamber.

34. Apply a small amount of grease to the rod and attach it to the top cap.

35. Place pressure chamber over the sample. Make sure it fits in the groove on the base.

36. Place the top plate on top of the pressure chamber. Again, make sure that it fits in the groove of the top plate.

37. Put in the three stabilizing rods and tighten them down.

38. Tighten down the top plate to the rod.

39. Slowly open the air valve of the deaerator to remove any remaining air bubbles.

40. Shut off the vacuum pump.

41. Attach deaerator water tube to the central valve in the base. Keep the valve on the tube closed.

42. Attach a tube to the top plate.

43. Slowly open the valve in the deaerator again and leave it open.

44. Open the valve of water tube and begin to fill the pressure chamber. Attempt to remove air bubbles as they appear.

45. Once water starts to come out of the top tube, shut all valves and remove all water tubes.

46. Close off the valve where the vacuum tube is attached, then remove the vacuum tube.

APPENDIX C: CONE PENETRATION TEST SET UP

C.1 Equipment

- Membrane

- O-rings x 6

- Porous stone x 1

- Filter paper x 2

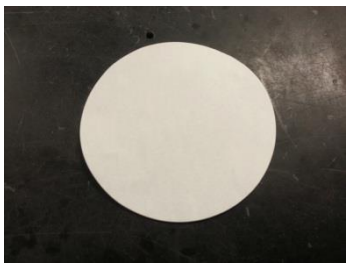

- Base

- Top cap

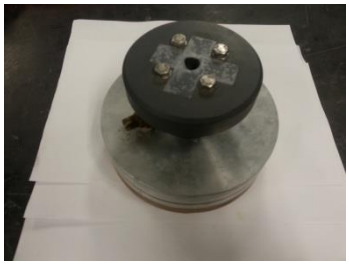

- Mold

- Mold clamp x 2

- Pressure chamber

- Cone Penetrometer

- Securing Plate

- Lead Screws x 2

- Support rod x 4

C.2 Instructions for Setting Up The Cone Penetration Test On Dry, Granular Sample

1. Apply vacuum grease around the groove on the top cap, the groove on the base and six o-rings.

2. Put the membrane on the base such that the bottom of the membrane is flush with the lower surface of the base.

3. Apply three of the o-rings to secure the membrane to the base. One o-ring should be in the groove with two o-rings below it.

4. Wipe down the inside of the mold halves.

5. Apply grease down the contact surfaces of both mold halves.

6. Place the mold around the membrane. Make sure that the membrane is not pinched by the mold.

7. Place the mold clamps around the mold on the top and bottom, and then tighten the nuts down.

8. Fold the membrane over the mold.

9. Weigh the current setup with all of the parts (top cap, rest of the o-rings with grease, porous stone, and filter paper.

10. Apply vacuum to the mold. Use up to 20 kPa.

11. Place a porous stone in the membrane such that it is flush with the bottom.

12. Put filter paper on top of the stone.

13. Place on respirator.

14. Weigh out each soil layer and pour into membrane. Tap down soil layers if necessary.

15. Place filter paper on top of soil.

16. Place top cap on top of the stone.

17. Fold up the membrane.

18. Place the remaining o-rings around the top cap.

19. Sweep around the base of the mold.

20. Attach tubes to the top cap.

21. Seal off the vacuum and remove the vacuum tube.

22. Apply two strips of tape over the hole on the top cap.

23. Weigh the final setup.

24. Hook up vacuum to the left most valve on the base. Make sure the middle two valves are open and the right most valve is closed. Vacuum should be under 20 kPa.

25. Remove the mold.

26. Measure the diameter of the sample in four places.

27. Measure the height of the sample in four places.

28. Place pressure chamber over the sample. Make sure the top cap fits inside the cavity at the top of the pressure chamber.

29. Put in the four stabilizing rods and tighten them down.

30. Place the cone penetrometer on top of the pressure chamber and secure it with the securing plate and lead screws.

APPENDIX D: BENDER ELEMENT TEST SET UP

D.1 Equipment

- Membrane

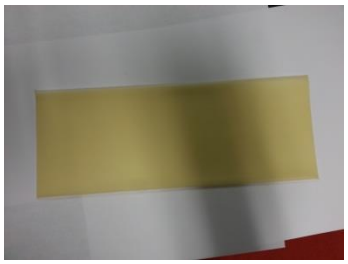

- O-rings x 6

- Base and Top Cap Assembly

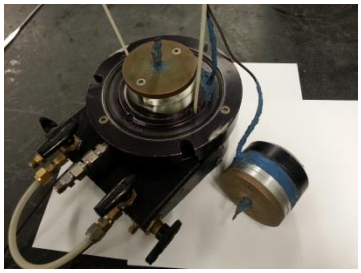

- Mold

- Mold clamp

- Collection Pan

- Pressure chamber

- Piston

- Support rod x 3

D.2 Instructions for Setting Up Bender Element Sample Apparatus

1. Apply vacuum grease around the groove on the top cap, the groove on the base and six o-rings.

2. Put the membrane on the base such that the bottom of the membrane is flush with the lower surface of the base.

3. Apply three of the o-rings to secure the membrane to the base. One o-ring should be in the groove with two o-rings below it.

4. Wipe down the inside of the mold halves.

5. Apply grease down the contact surfaces of both mold halves.

6. Place the mold around the membrane. Make sure that the membrane is not pinched by the mold.

7. Place the mold clamp around the mold and tighten the nut down.

8. Place the remaining three o-rings around the top of the mold.

9. Fold the membrane over the mold.

10. Weigh the current setup with all of the top parts (top cap, rest of the o-rings with grease, porous stone, filter paper.

11. Remove from scale and put on the collection pan.

12. Apply vacuum to the mold. Use up to 20 kPa.

13. Place on respirator.

14. Weigh out each soil layer and pour into membrane. Tap down soil layers if necessary.

15. When all soil is in membrane, remove the collection pan.

16. Place top cap on top of the soil.

17. Fold up the membrane.

18. Slide the remaining o-rings up around the top cap.

19. Sweep around the base of the mold.

20. Attach tubes to the top cap.

21. Seal off the vacuum and remove the vacuum tube.

22. Weigh the final setup.

23. Hook up vacuum to the left most valve on the base. Make sure the middle two valves are open and the right most valve is closed. Vacuum should be under 12 kPa.

24. Remove the mold.

25. Measure the diameter of the sample in four places.

26. Measure the height of the sample in four places.

27. Apply grease to the top and bottom of the pressure chamber.

28. Apply a small amount of grease to the rod and attach it to the top cap.

29. Place pressure chamber over the sample. Make sure it fits in the groove on the base.

30. Place the top plate on top of the pressure chamber. Again, make sure that it fits in the groove of the top plate.

31. Put in the three stabilizing rods and tighten them down.

32. Tighten down the top plate to the rod.

33. Move setup to the bender element machine.

34. Attach the compressed air hose to the valve in the top plate. Apply the lowest air pressure of 12.5 kPa while slowly letting out the vacuum in the sample.

COMPREHENSIVE BIBLIOGRAPHY

Allen, C., Lindstrom, R., Lindstrom, M,, and Lockwood, J. (1997) "JSC MARS-1: MARTIAN REGOLITH SIMULANT." *Lunar and Planetary Science XXVIII*

Alshibli, K., and Hasan, A. (2009) "Strength Properties of JSC-1A Lunar Regolith Simulant." *Journal of Geotechnical and Geoenvironmental Engineering* 135.5: 673.

Alshibli, K., and Sture, S. (2000) "Shear Band Formation in Plane Strain Experiments of Sand." *Journal of Geotechnical and Geoenvironmental Engineering* 126.6: 495.

ASTM D2425 (1991) "Standard Test Methods for One-Dimensional Consolidation Properties of Soils Using Incremental Loading"

ASTM D854 (1991) "Standard Test Methods for Specific Gravity of Soils by Water Pyncnometer"

ASTM D4253 (2006) "Standard Test Methods for Maximum Index Density and Unit Weight of Soils Using a Vibratory Table."

ASTM D4254 (2006) (Standard Test Methods for Minimum Index Density and Unit Weight of Soils and Calculation of Relative Density)

ASTM D2850 (2007) "Standard Test Methods for Unconsolidated-Undrained Triaxial Compression Test for Cohesive Soils"

ASTM D6913 (2009) "Standard Test Methods for Particle-Size Distribution (Gradation) of Soils Using Sieve Analysis"

Bekker, M. G. *Introduction to Terrain-vehicle Systems*. Ann Arbor: U of Michigan, 1969.

Bekker, M. G. *Theory of Land Locomotion; the Mechanics of Vehicle Mobility*. Ann Arbor: U of Michigan, 1956.

Bin, C., Jianqio, L., Yinwu, L., "Pressure-sinkage Model and Experimental Research of Interaction Between Rigid-wheel and Simulant Lunar Soil". *Intelligent Vehicles Symposium*, 2009.

Blewett, J., Blewett, I.j., and Woodward, P.k. (2000) "Phase and Amplitude Responses Associated with the Measurement of Shear-wave Velocity in Sand by Bender Elements." *Canadian Geotechnical Journal* 37.6: 1348-357.

Bolton, M. D. (1986) "The Strength and Dilatancy of Sands." *Géotechnique* 36.1: 65-78.

Bolton, M. D., Gui, M. W., Garnier, J., Corte, J. F., Bagge, G., Laue, J., and Renzi, R. "Centrifuge cone penetration tests in sand", *Geotechnique*; 1999, 49(4), 543-552.

Brunskill, C., Patel, N, Gouache, T. P., Scott, G. P., Saaj, C. M., Matthews, M., and Cui, L. "Characterisation of Martian Soil Simulants for the ExoMars Rover Testbed." *Journal of Terramechanics*; 2011, 48.6: 419-38

Budhu, M. Soil Mechanics and Foundations, John Wiley & Sons, Inc., 2nd edition; 2007.

Chaney, R., Demars, K., Brignoli, E., Gotti, M., and Stokoe, K. (1996) "Measurement of Shear Waves in Laboratory Specimens by Means of Piezoelectric Transducers." *Geotechnical Testing Journal* 19.4: 384.

Duncan, C. I. *Soils and Foundations for Architects and Engineers*. 2nd ed. New York: Van Nostrand Reinhold; 1998.

Dyvik, R., and Madshus, C. (1985) "Lab Measurements of G_{max} Using Bender Elements." *Advances in the Art of Testing Soils under Cyclic Conditions: Proceedings of a*

Session. By Vijay Khosla. New York, NY: American Society of Civil Engineers.

Edmunson, J. (2010) “Simulant Listing” *NASA - In Situ Resource Utilization*.

Edwards, M., Dewoolkar, M., Huston, D. “Geotechnical Propertied of Fillite – a Simulant for High-Slip/High Sinkage Rover Mobility Studies.” *Journal of Aerospace Engineering.* Currently under review; 2014.

Fang, H.-Y. (1990), Foundation Engineering Handbook, 2nd ed., Kluwer Academic Publishers.

Goriatchkin, B. "Teoria I Proisvodstvo Sielskohoziaynih Mashin." *Collective Work*; 1937.

Gotteland, P., and Benoit, O. "Sinkage Tests for Mobility Study, Modelling and Experimental Validation." *Journal of Terramechanics*; 2006, 43.4: 451-67.

Janosi, Z., Hanamoto, B., "*The Analytical Determination of Drawbar Pull as a Function of Slip for Tracked Vehicles in Deformable Soils*", Proceedings of the 1st International Conference on the Mechanics of Soil-Vehicle Systems, Edizioni Minerva Tecnica, Torino, Italy; 1961.

Hardin, B. O., and Richart, F. E. (1963) "Elastic Wave Velocities in Granular Soils." *Journal of Soil Mechanics and Foundations Division* 33.1: 33-65.

He, C., Zeng, X., and Wilkinson, A. (2011) "Geotechnical Properties of GRC-3 Lunar Simulant." *Journal of Aerospace Engineering* 26: 528-534

Heiken, G., Vaniman, D., and French, B. (1991) *Lunar Sourcebook: A User's Guide to the Moon*. Cambridge: Cambridge UP.

Katagiri, M., and Okamura, M. “Manual of basic centrifuge tests, 4. Cone penetration test, Proc. International Conference *Centrifuge 9;* 2000, Vol. 2, 1059-1066.

Kulhway, F.H. and Mayne, P.W. (1990) “Manual on Estimating Soil Properties for Foundation Design.” *Report EPRI EL-6800,* Prepared for Electric Power Research Institute.

Lee, J-S., and Santamarina, J. (2005) "Bender Elements: Performance and Signal Interpretation." *Journal of Geotechnical and Geoenvironmental Engineering* 131.9: 1063.

Li, Y., Zeng, X., and Agui, J. (2013) "Developing a Light Weight Martian Soil Simulant (CWRU1) for High Sinkage Mobility Test." *Journal of Aerospace Engineering*: 130807091030006.

Lindemanne, R., "*Broader Interests and Applications: The view of a JPL Hardware Engineer",* XTerramechanics: Integrated Simulation of Planetary Surface Missions, CalTech; 2011

Mayne, P. W., Christopher, B. R., DeJong, J., “Subsurface Investigations – Geotechnical site Characterization”. *National Highway Institute*; 2002, pg 9-12 to 9-15. Publication No. FHWA NHI-01-31

McKee, Maggie. "Mars rover may not escape sand trap for weeks". *New Scientist*. May 12, 2009.

Moore, H. J., Clow, G. D., and Hutton, R. E. (1982) "A Summary of Viking Sample-Trench Analyses for Angles of Internal Friction and Cohesions." *Journal of Geophysical Research* 87.B12: 10043-0050.

Meirion-Griffith, G., and Spenko, M. "A Modified Pressure–sinkage Model for Small, Rigid Wheels on Deformable Terrains." *Journal of Terramechanics*; 2011 48.2:149-55.

Moore, H., and Jakosky, B. (1989) "Viking Landing Sites, Remote-sensing Observations, and Physical Properties of Martian Surface Materials." *Icarus* 81.1: 164-84.

Moore, H., Bickler, D., Crisp, J., Eisen, H., Gensler, J., Haldemann, A., Matijevic, J., Reid, L., and Pavlics, F. (1999) "Soil-like Deposits Observed by Sojourner, the Pathfinder Rover." *Journal of Geophysical Research* 104.E4: 8729-746.

NASA, "Spirit and Opportunity Mission News", http://www.nasa.gov/mission_pages/mer/freespirit.html, 2009. Last accessed August 6, 2014.

NASA, (2009) "Spirit Rover Mission Update, Sol 1900-1906." http://mars.jpl.nasa.gov/mer/mission/status_spiritAll_2009.html#sol2100

Oravec, Heather Ann. *Understanding Mechanical Behavior of Lunar Soils for the Study of Vehicle Mobility*. Thesis. Case Western Reserve University, 2009.

Oravec, H. A., Zeng, X., and Asnani, V. M. (2010) "Design and Characterization of GRC-1: A Soil for Lunar Terramechanics Testing in Earth-ambient Conditions." *Journal of Terramechanics* 47.6: 361-77

Peters, G. H., Gregory, W. A., Bearman, H., Mungas, G.S., Smith, J., Anderson, R. C., Douglas, S., and Beegle, L. W. "Mojave Mars Simulant—Characterization of a New Geologic Mars Analog." *Icarus,*; 2008, 197.2 : 470-79.

Peters, G., Abbey, W., Bearman, G., Mungas, G., Smith, A., Anderson, R., Douglas, S. and Beegle, L. (2008) "Mojave Mars Simulant—Characterization of a New Geologic Mars Analog." *Icarus* 197.2: 470-79.

Robertson, P.K. and Campanella R. G. "Interpretation of cone penetration tests: PartI – sands; part II – clays". *Canadian Geotechnical Journal*; 1983, Vol. 20 (4), 719-745.

Seiferlin, K., Ehrenfreund, P., Garry, J., Gunderson, K., Hütter, E., Kargl, G., Maturilli, A., and Merrison, J. (2008) "Simulating Martian Regolith in the Laboratory." *Planetary and Space Science* 56.15: 2009-025.

Sirles, P. C., and Viksne, A. (1990) "Site-Specific Shear Wave Velocity Determinations for Geotechnical Engineering Applications". *Geotechnical and Environmental Geophysics, Investigations in Geophysics No. 5, Society of Exploration Geophysicists*, Tulsa, OK, pp 121-131.

Stoker, C.R., Gooding, J.L., and Roush, T. (1993) "The Physical and Chemical Properties and Resource Potential of Martian Surface Soils." *Resources of Near-Earth Space*. By Banin, A., D. Burt, and B.C. Clarke. Tucson: U of Arizona.

Sullivan, R., Anderson, R., Biesiadecki, J., Bond, T., and Stewart, H. (2011) "Cohesions, Friction Angles, and Other Physical Properties of Martian Regolith from Mars Exploration Rover Wheel Trenches and Wheel Scuffs." *Journal of Geophysical Research* 116.E2. DOI: 10.1029/2010JE003625

Tolsa USA Inc, http://www.thecarycompany.com/products/Tolsa/tolsa-usa-inc-fillite.html, last accessed: July 5,2014

Trease, B., Arvidson, R., Lindemann, R., Bennett, K., Zhou, F., Iagnemma, K., Senatore, C., Van Dyke, L. “Dynamic modeling and soil mechanics for path planning of Mars Exploration Rovers.” Paper presented at the *ASME Design Engineering Technical Conference*, Washington, DC; 2011.

Vermeer, P. A., and Schanz, T. (1996) "Angles of Friction and Dilatancy of Sand." *Géotechnique* 46.1: 145-51.

Viggiani, G., and Atkinson, J.h. (1995) "Stiffness of Fine-grained Soil at Very Small Strains." *Géotechnique* 45.2: 249-65.

Wong, J., & Reece, A. *"Prediction of Rigid Wheel Performance Based on the Analysis of Soil-wheel Stresses. Part I. Performance of Driven Rigid Wheels*". Journal of Terramechanics; 1967, 4(1), 81–98

Wong, J.y. "Data Processing Methodology in the Characterization of the Mechanical Properties of Terrain." *Journal of Terramechanics*; 1980, 17.1 : 13-41.

Wong, J. Y. “Terramechanics and Off-road Vehicle Engineering: Terrain Behaviour, Off-road Vehicle Performance and Design”. *Amsterdam: Butterworth-Heinemann*; 2010.